



HAL
open science

Magnetic Holes in the Solar Wind and Magnetosheath Near Mercury

T. Karlsson, D. Heyner, M. Volwerk, M. Morooka, F. Plaschke, C. Goetz, L.
Hadid

► **To cite this version:**

T. Karlsson, D. Heyner, M. Volwerk, M. Morooka, F. Plaschke, et al.. Magnetic Holes in the Solar Wind and Magnetosheath Near Mercury. *Journal of Geophysical Research Space Physics*, 2021, 126 (5), pp.e2020JA028961. 10.1029/2020ja028961 . hal-03260558

HAL Id: hal-03260558

<https://hal.sorbonne-universite.fr/hal-03260558>

Submitted on 15 Jun 2021

HAL is a multi-disciplinary open access archive for the deposit and dissemination of scientific research documents, whether they are published or not. The documents may come from teaching and research institutions in France or abroad, or from public or private research centers.

L'archive ouverte pluridisciplinaire **HAL**, est destinée au dépôt et à la diffusion de documents scientifiques de niveau recherche, publiés ou non, émanant des établissements d'enseignement et de recherche français ou étrangers, des laboratoires publics ou privés.



Magnetic Holes in the Solar Wind and Magnetosheath Near Mercury

T. Karlsson¹ , D. Heyner² , M. Volwerk³ , M. Morooka⁴ , F. Plaschke³ , C. Goetz⁵ , and L. Hadid⁶

Key Points:

- We present a comprehensive statistical study of magnetic holes in the near-Mercury solar wind and magnetosheath
- We find that magnetic hole scale sizes are log-normally distributed
- We suggest that a majority of the magnetosheath magnetic holes have a solar wind origin

¹Division of Space and Plasma Physics, School of Electrical Engineering and Computer Science, KTH Royal Institute of Technology, Stockholm, Sweden, ²Space Research Institute, Austrian Academy of Sciences, Graz, Austria, ³Institute for Geophysics and Extraterrestrial Physics, Technische Universität Braunschweig, Braunschweig, Germany, ⁴Swedish Institute of Space Physics, Uppsala, Sweden, ⁵ESA/ESTEC SCI-S, Noordwijk, the Netherlands, ⁶Laboratoire de Physique des Plasmas, CNRS-Ecole Polytechnique-Sorbonne Université-Univ. Paris-Saclay-Observatoire de Paris-Meudon, Palaiseau, France

Correspondence to:

T. Karlsson,
tomas.karlsson@ee.kth.se

Citation:

Karlsson, T., Heyner, D., Volwerk, M., Morooka, M., Plaschke, F., Goetz, C., & Hadid, L. (2021). Magnetic holes in the solar wind and magnetosheath near Mercury. *Journal of Geophysical Research: Space Physics*, 126, e2020JA028961. <https://doi.org/10.1029/2020JA028961>

Received 24 NOV 2020

Accepted 29 APR 2021

Abstract We present a comprehensive statistical study of magnetic holes, defined as localized decreases of the magnetic field strength of at least 50%, in the solar wind near Mercury, using MESSENGER orbital data. We investigate the distributions of several properties of the magnetic holes, such as scale size, depth, and associated magnetic field rotation. We show that the distributions are very similar for linear magnetic holes (with a magnetic field rotation across the magnetic holes of less than 25°) and rotational holes (rotations >25°), except for magnetic holes with very large rotations (≥140°). Solar wind magnetic hole scale sizes follow a log-normal distribution, which we discuss in terms of multiplicative growth. We also investigate the background magnetic field strength of the solar wind surrounding the magnetic holes, and conclude that it is lower than the average solar wind magnetic field strength. This is consistent with finding solar wind magnetic holes in high-β regions, as expected if magnetic holes have a connection to magnetic mirror mode structures. We also present, for the first time, comprehensive statistics of isolated magnetic holes in a planetary magnetosheath. The properties of the magnetosheath magnetic holes are very similar to the solar wind counterparts, and we argue that the most likely interpretation is that the magnetosheath magnetic holes have a solar wind origin, rather than being generated locally in the magnetosheath.

1. Introduction

Solar wind magnetic holes were first reported by Turner et al. (1977) using magnetic field data from the Explorer 43 (IMP-6) spacecraft, and were defined as “isolated regions in the form of distinct depressions, or ‘holes’ in otherwise nearly average conditions.” Such magnetic holes have since then been studied by many authors, at various heliocentric distances. We stress here that we will use the original definition of Turner et al. (1977) that the magnetic holes be isolated, and not a part of a quasi-periodic train as seen in observations of mirror mode waves (e.g., Chisham et al., 1999; Soucek et al., 2008; Volwerk et al., 2008). This definition has been used also by for example, Neugebauer et al. (2001) and Stevens and Kasper (2007).

The temporal scale sizes of magnetic holes have been reported to vary between a few seconds and several minutes (Madanian et al., 2019; Sperveslage et al., 2000; Turner et al., 1977; Volwerk et al., 2020; Winterhalter et al., 1994; Xiao et al., 2010; Zhang, Russell, Baumjohann, et al., 2008). The variation of scale size with heliocentric distance is unclear. Volwerk et al. (2020) found no change in typical scale sizes between 0.3 and 0.7 AU, and their reported typical scale sizes of 4–30 s are consistent with Xiao et al.’s (2010) results of a mean of 10 s (as measured in the direction along the background magnetic field) at 1 AU. On the other hand Turner et al. (1977) gives a median of 50 s at 1 AU, while Madanian et al. (2019) reports a median of 19 s at 1.5 AU. Finally, Sperveslage et al. (2000) find an increase from an average scale size of 8 s in the inner solar system to 32 s for 2–17 AU (while pointing out that normalized to proton gyro radii, the scale sizes actually decrease with heliocentric distance.) This somewhat unclear situation may be due to slightly varying definitions of magnetic hole identification and scale sizes. It would be desirable to use consistent measures and not only give simple measures as means or medians, but to compare full distributions of scale

© 2021. The Authors.

This is an open access article under the terms of the [Creative Commons Attribution-NonCommercial-NoDerivs](https://creativecommons.org/licenses/by/4.0/) License, which permits use and distribution in any medium, provided the original work is properly cited, the use is non-commercial and no modifications or adaptations are made.

sizes (and other properties). Such distributions may also give clues to generation mechanisms, and act as strong constraints on theories of magnetic hole origin.

Turner et al. (1977) suggested that there are two types of magnetic holes: one associated with a clear rotation of the magnetic field from one side of the hole to the other (“rotational” magnetic holes), and one type without such a rotation (“linear” holes). This has been verified in several studies (Briand et al., 2010; Madanian et al., 2019; Sperveslage et al., 2000; Tsurutani et al., 2009; Volwerk et al., 2020; Winterhalter et al., 1994; Xiao et al., 2010; Zhang, Russell, Baumjohann, et al., 2008; Zhang, Russell, Zambelli, et al., 2008) at various heliocentric distances. Various definitions of linear magnetic holes have been employed, but a commonly used definition is that the angle between the magnetic field direction before and after the magnetic hole be less than 10° (Briand et al., 2010; Madanian et al., 2019; Sperveslage et al., 2000; Tsurutani et al., 2011; Volwerk et al., 2020). On the other hand Briand et al. (2010) and Xiao et al. (2010) use a limit of 15° , while Zhang et al. define linear magnetic holes to have an angular change of less than 10° , while requiring a rotational hole to have an angular change of at least 30° (Zhang, Russell, Baumjohann, et al., 2008; Zhang, Russell, Zambelli, et al., 2008).

The daily occurrence rate of magnetic holes as a function of heliocentric distance is also unclear. In the inner solar system, Volwerk et al. (2020) found a decrease from 3.4 d^{-1} at 0.3 AU to 2.4 d^{-1} at 0.7 AU for linear magnetic holes (“ d^{-1} ” is “per day”), while magnetic holes with larger rotations had a constant occurrence rate. Xiao et al. (2010), on the other hand, give an occurrence rate of 3.7 d^{-1} for linear holes at 1 AU. Sperveslage et al. (2000) conclude that there is no dependence on distance between 0.3 AU and 1 AU. They do, however, report on a decrease from 0.5 d^{-1} (2–4 AU) to 0.1 d^{-1} (beyond 11 AU). At 1.7 AU (at Mars orbit) Madanian et al. (2019) give a rate of 2.1 d^{-1} (including both linear and rotational magnetic holes).

Magnetic holes have been found to typically exist in a balance between magnetic and thermal pressure (Madanian et al., 2019; Neugebauer et al., 2001; Stevens & Kasper, 2007; Winterhalter et al., 1994). This is also a typical property of magnetic mirror mode structures (e.g., Hasegawa, 1969), which has motivated several authors to suggest a connection between linear magnetic holes and the mirror mode instability, especially since mirror mode structures typically have a linear polarization (Tsurutani et al., 2011, and references therein). As support for this idea several authors (Madanian et al., 2019; Stevens & Kasper, 2007; Winterhalter et al., 1994) also cite the fact that magnetic holes are often found in regions where the solar wind plasma is either unstable or only marginally stable with respect to the mirror mode instability criterion (e.g., Southwood & Kivelson, 1993):

$$1 + \beta_{\perp} \left(1 - \frac{T_{\perp}}{T_{\parallel}} \right) < 0, \quad (1)$$

where β_{\perp} is the ratio of the perpendicular thermal pressure to magnetic pressure, and T_{\perp} and T_{\parallel} are the perpendicular and parallel temperatures.

Magnetic holes also tend to occur in solar wind regions with higher β than in the average solar wind (Sperveslage et al., 2000; Winterhalter et al., 1994), where the mirror mode instability may dominate over the competing ion cyclotron instability (e.g., Schwartz et al., 1997, and references therein). Winterhalter et al. (1994) suggest a scenario in which magnetic holes are remnants of solar wind magnetic mirror mode structures, possibly having undergone non-linear interactions such as coalescing, while the solar wind plasma has also relaxed to a marginally stable state (Stevens & Kasper, 2007). Another possibility is that single magnetic holes may be the result of the plasma being marginally unstable, perhaps in such a small region that only a single structure is growing, instead of a train of holes. It has also been suggested that magnetic holes can continue to propagate in the solar wind as soliton structures, even in a mirror mode stable environment (Baumgärtel, 1999; Sperveslage et al., 2000).

However, also other theories for the generation of linear magnetic holes have been put forward. Several authors suggest non-linear evolution of Alfvén waves as a generation mechanism. Buti et al. (2001) suggest that large-amplitude, right-handed polarized Alfvén wave packets propagating almost perpendicular to the magnetic field can develop into magnetic holes, with no or little temperature anisotropy, while Tsurutani, Dasgupta, et al., 2002; Tsurutani, Galvan, et al., 2002) suggest that ion heating due to the ponderomotive

force of phase steepened Alfvén waves produces the magnetic holes via a diamagnetic response. Another class of models describe magnetic holes as soliton solutions in fluid models (Avinash & Zank, 2007; Baumgärtel, 1999; Stasiewicz et al., 2003). Finally, magnetic holes have also been suggested to form as emergent coherent structures in solar wind turbulence (Perrone et al., 2016, 2017; Roytershteyn et al., 2015).

Regarding rotational magnetic holes, their generation has been little discussed. Neugebauer et al. (2001) and Zurbuchen et al. (2001) argue against their being remnants of structures created in the photosphere, since they do not show any difference in chemical composition to the surrounding solar wind. Instead, it has been suggested that rotational magnetic holes are the result of flux annihilation due to slow reconnection at the current sheets associated with the magnetic field rotation (Turner et al., 1977; Zhang, Russell, Baumjohann, et al., 2008).

The effects of magnetic holes, and their interaction with the space environment of planets and other celestial bodies is poorly known and little studied. Modeling work by Wu et al. (1993) and Grib and Leora (2015) indicates that magnetic holes can cross the bow shock, after being compressed and modified, and continue to convect with the magnetosheath flow. In a small study of “diamagnetic plasmoids” in Earth’s magnetosheath, using Cluster data, Karlsson et al. (2012) and Karlsson et al. (2015) showed that these structures were localized increases in density, anti-correlated with magnetic field strength. Their properties were very similar to analogous structures found in the solar wind, which were proposed to be examples of solar wind magnetic holes, albeit with a smaller magnetic field decrease than usually required in definitions of magnetic holes. The magnetosheath diamagnetic plasmoids were suggested to probably be solar wind magnetic holes that had crossed the bow shock. In a recent study, Parkhomov et al. (2019) using OMNI solar wind data identified structures that were likely the solar wind counterpart of the magnetosheath diamagnetic plasmoids measured by Cluster, thus supporting the scenario in which magnetic holes can enter the magnetosheath. Once in the magnetosheath, their increased momentum due to their higher density may affect the magnetosphere in similar way as magnetosheath jets (Plaschke, Hietala, et al., 2018), for example, triggering surface waves, reconnection and impulsive penetration. Also the different magnetic field inside the magnetic hole, as compared to outside of it, may locally affect reconnection processes. Karlsson et al. (2016) also performed a small statistical study of magnetic holes in the near-Mercury solar wind and magnetosheath, using MESSENGER magnetic field data, and found that magnetic holes in the two regions had similar properties, again indicating that solar wind magnetic holes seem to be able to penetrate the bow shock, although the statistical sample was rather small. Finally, Plaschke, Karlsson, et al. (2018) showed that magnetic holes could be found in the inner coma of comet 67P, even in regions where the solar wind ions were absent, showing that solar wind magnetic holes can penetrate deep into the surroundings of solar system bodies.

The purpose of this paper is two-fold. We will make a detailed investigation of the properties of solar wind magnetic holes close to Mercury, based on the whole magnetic field database from the orbital phase of the MESSENGER mission. This is done also as part of a long-ranging goal of revisiting data sets at different heliocentric distances to study the variation of magnetic hole properties using a consistent definition of what constitutes a magnetic hole. We will also look for magnetic holes in the magnetosheath of Mercury, and compare their properties to the solar wind magnetic holes, to investigate if they are consistent with solar wind magnetic holes crossing the bow shock, or if they are more likely to be created locally in the magnetosheath.

2. Data and Event Identification

We use magnetic field data from the MAG instrument onboard the MESSENGER spacecraft (Anderson et al., 2007). We exclusively use data sampled at 20 Hz, in the time range 2011-04-01–2015-04-29. This corresponds to about 2 weeks after orbit insertion (2011-03-18) to the end of mission by deorbiting at 2015-04-30. The only other plasma instrument onboard MESSENGER, the Fast Imaging Plasma Spectrometer (FIPS) had some serious limitations in that the sunshade and solar panels obstructed a large part of the field of view, particularly for the generally anti-sunward flows in the solar wind and magnetosheath. Consequently moment calculations are normally not possible to perform for data from the solar wind and magnetosheath where the bulk flow velocity is greater than or comparable to the thermal velocity (Raines et al., 2011).

We therefore base this study exclusively on magnetic field data, similar to the recent paper by Volwerk et al. (2020).

To identify magnetosheath and solar wind intervals in the data, we use the MAG team's identification of bow shock and magnetopause crossings, originally published by Winslow et al. (2013), and later extended by the MAG team (Philpott et al., 2020). From this we first determine intervals when MESSENGER is situated in the solar wind or the magnetosheath. For each such interval, we look for magnetic hole candidates by first determining a background level of the magnetic field strength, B_0 . This is determined by calculating the mean (indicated by angular brackets) of the magnitude of the magnetic field $|\mathbf{B}|$, with a sliding window with a width of 300 s:

$$B_0 = \langle |\mathbf{B}| \rangle_{300\text{s}}. \quad (2)$$

We then calculate the relative deviation $\frac{\Delta B}{B_0}$ from this background level by subtracting it from the original time series of $|\mathbf{B}|$, and dividing by the background level. We finally smooth the resulting signal by a 1 s sliding window, to remove high-frequency variations, and we have

$$\frac{\Delta B}{B_0} = \left\langle \frac{|\mathbf{B}| - B_0}{B_0} \right\rangle_{1\text{s}}. \quad (3)$$

We furthermore calculate the standard deviation σ_B of $|\mathbf{B}|$ averaging it in a 300 s running window, and normalize it to the background magnetic field

$$\sigma_{B,norm} = \frac{\langle \sigma_B \rangle_{300\text{s}}}{B_0}. \quad (4)$$

We use the normalized standard deviation to exclude regions of oscillations and turbulence in the solar wind associated with the foreshock (Jarvinen et al., 2019; Le et al., 2013; Uritsky et al., 2011). There are two reasons for this. First, we want to make sure that we study magnetic holes that are created in the pristine solar wind, and exclude possible depressions in magnetic field strength created in the disturbed solar wind close to the planet. Second, it is very difficult to identify isolated magnetic holes in the turbulent environment of the foreshock. A similar technique was used by Plaschke, Karlsson, et al. (2018) to find isolated magnetic holes in the coma of comet 67P. By a trial-and-error method, including visual identification of foreshock regions, we have set a limit of $\sigma_{B,norm} < 0.05$ for including solar wind data in the search of magnetic holes.

We apply the same criterion in the magnetosheath, $\sigma_{B,norm} < 0.05$, both to increase the likelihood of identifying clean events, and to exclude the large-amplitude, embedded pulsations found behind the quasi-parallel bow shock (Sundberg et al., 2013, 2015).

A magnetic hole candidate event is then defined as a series of data points with $\frac{\Delta B}{B_0} < -50\%$, with the start-time of the event taken as the sample time of the first data point fulfilling the criterion, and the end time corresponding to the last data point in the series. In order to identify isolated magnetic holes, we demand that for an isolated magnetic hole, no other magnetic hole candidate data point with $\sigma_{B,norm} < 0.05$ is found within 60 s of either the start or end time of the candidate event.

3. Results

The above procedure resulted in the identification of 2,726 isolated solar wind magnetic holes, and 2,154 events in the magnetosheath. We have visually inspected all events, and these numbers are the result of discarding a few (<10) events that were affected by data gaps which disturbed the calculation of the background magnetic field.

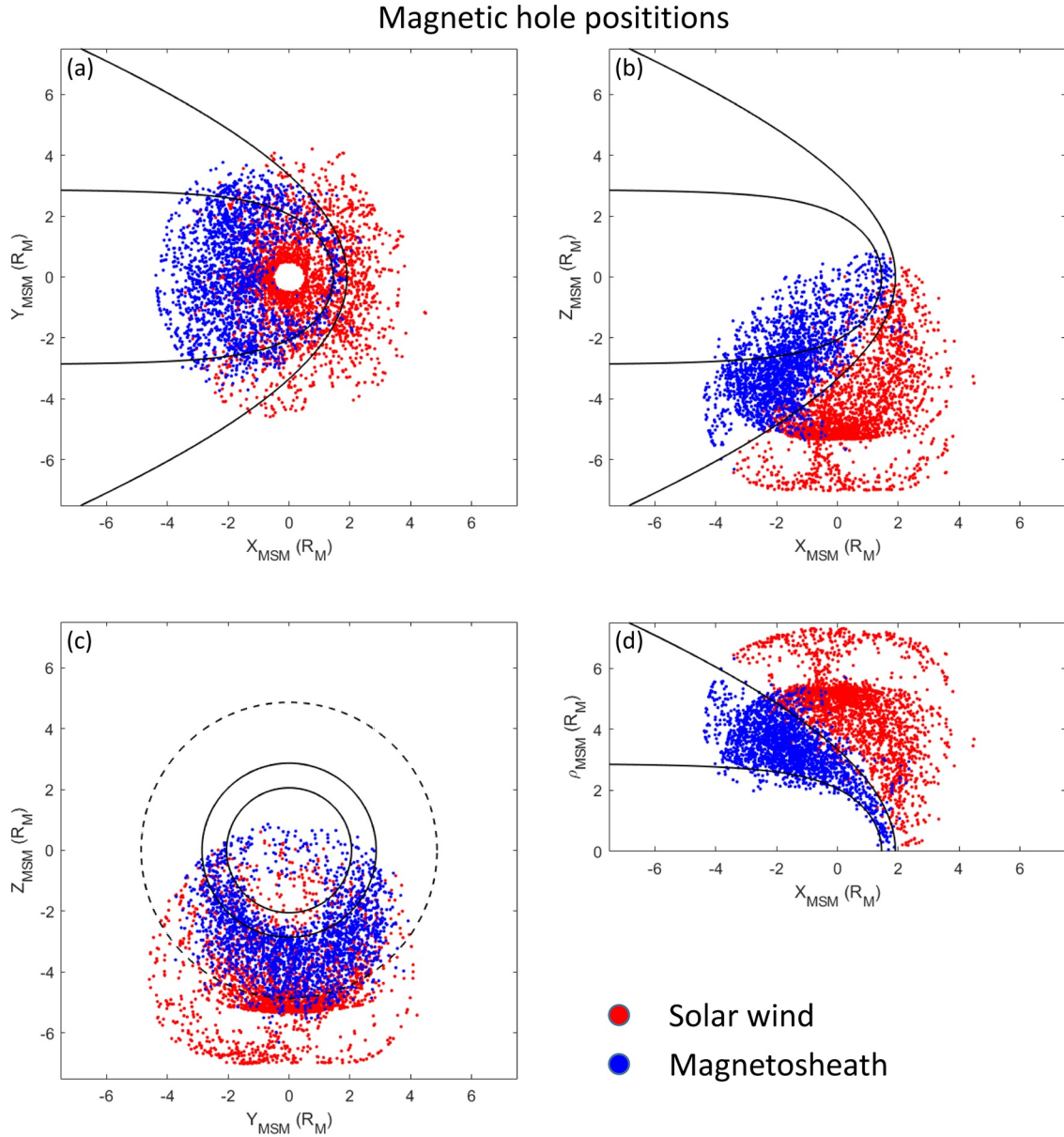


Figure 1. Positions of magnetic holes found in the solar wind and magnetosheath, in the MSM coordinate system. Indicated are model bow shock and magnetopause using parameters from Winslow et al. (2013). In panel (c) the bow shock is indicated for $X_{\text{MSM}} = -2 R_M$ with the broken line, while the bow shock and magnetopause for $X_{\text{MSM}} = 0$ are given by the solid lines.

The total observation times in the solar wind and magnetosheath (excluding times with $\sigma_{B, \text{norm}} \geq 0.05$) are 14,832 h, and 3 823 h, respectively. This means that the rate of observation of magnetic holes by MESSENGER is 4.4 d^{-1} and 17 d^{-1} , in the solar wind and magnetosheath, respectively.

The positions of all the identified magnetic holes are shown in Figure 1, using the MSM (Mercury Solar Magnetospheric) coordinate system. This system has the origin offset from the planetary center by the magnetic dipole offset, with x_{MSM} directed toward the sun, and z_{MSM} northwards. y_{MSM} completes the right-handed orthogonal system. Shown in panel (d) are also the positions in the $\rho_{\text{MSM}} - x_{\text{MSM}}$ projection, where $\rho_{\text{MSM}} = \sqrt{y_{\text{MSM}}^2 + z_{\text{MSM}}^2}$, where it is seen that the statistical bow shock and magnetopause sort the data well. We note that the magnetosheath coverage extends to about $-4 R_M$ (Mercury radii) in the anti-solar direction. The effect of the apoherm reduction in April 2012 can be clearly made out in panels (b)–(d).

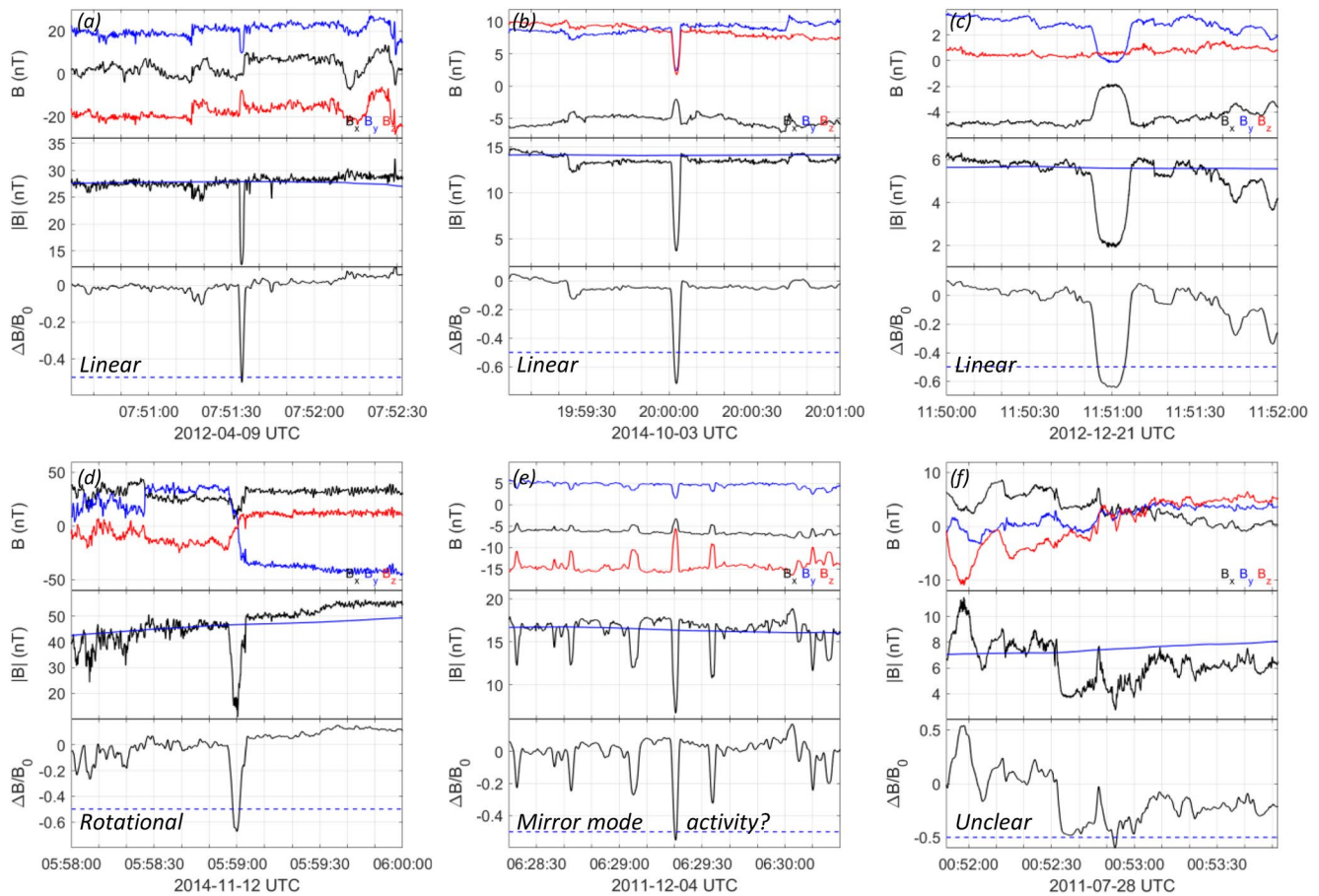


Figure 2. Representative examples of magnetic holes in the solar wind near Mercury. For each subplot is shown, from top to bottom, magnetic field components in the MSM coordinate system, magnitude of the magnetic field (black) with the calculated background field, B_0 (blue), and $\frac{\Delta B}{B_0}$ with the limit of -0.5 indicated by the dotted line. See text for explanation of the various types.

In Figure 2 we show a number of representative events from the solar wind. Panels (a) and (b) show two examples of linear magnetic holes with temporal scale sizes of a few seconds. This represents the most common type of observed solar wind magnetic holes (This and other properties discussed here will be quantified below by statistical analysis.) Panel(c) shows a similar magnetic hole, but with a larger scale size. Panel (d) is an example of a rotational magnetic hole. These are less common than the linear ones, but are not rare.

In a few cases the identified isolated magnetic holes are actually part of a short train of lower amplitude magnetic holes. An example is shown in panel (e). The magnetic hole at 06:29:20 UTC is identified as an isolated magnetic hole, since it is the only magnetic depression that fulfills the criterion of a 50% decrease of the magnetic field strength. This type of event is quite rare. The quasi-periodic appearance of the train of holes leads us to a preliminary identification of these structures as mirror mode waves (e.g., Chisham et al., 1999; Soucek et al., 2008; Volwerk et al., 2008), as discussed briefly in the Introduction.

Finally, we show an example of an identified event, (f), which does not have a clear structure in the way of the events in panels (a)–(e), but rather represents a more or less random excursion below the limit of 50% decrease. Such events are rare, but we show it in the interest of completeness.

In Figure 3, we show a similar selection of events from the magnetosheath. They are representative for the magnetosheath magnetic holes, in a similar way as for the solar wind holes: panels (a)–(b) show the most common type of magnetic holes, small-scale linear holes, while panel (c) is an example of a larger-scale linear hole. Panel (d) shows an example of a rotational whole. In panel (e), we show one of the trains of

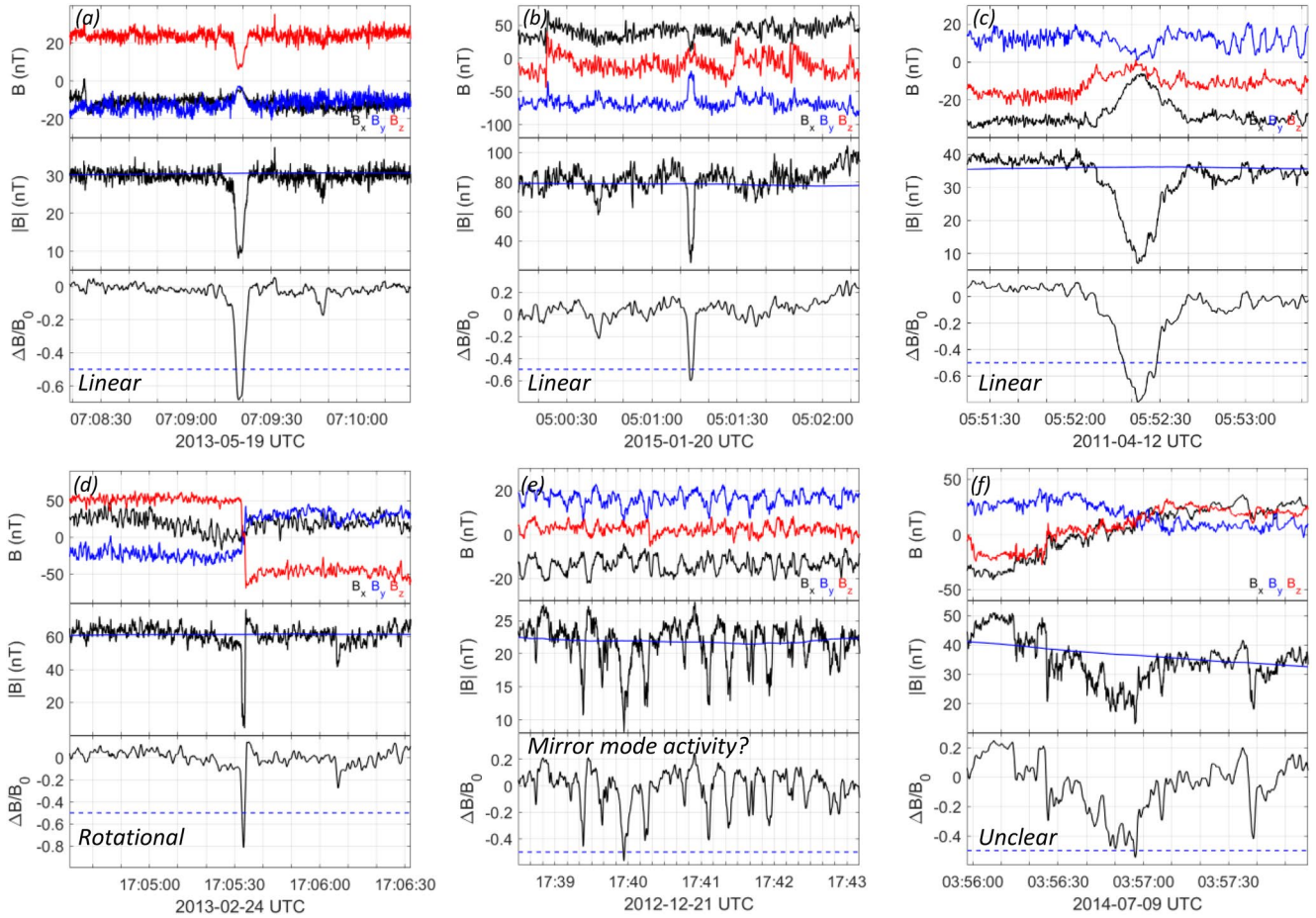


Figure 3. Representative examples of magnetic holes in the magnetosheath of Mercury, in the same format as in Figure 2.

holes that sometimes, but rarely, also occur in the Hermean magnetosheath. Finally, in panel (f) is shown a rare irregular/unclear event.

We now move on to investigate the properties of the solar wind and magnetosheath magnetic holes in more detail. We first consider the rotation of the magnetic field over the magnetic hole. We determine this by averaging the magnetic field vector components on each side of the hole. Before the hole we average over a time period

$$t_{av} \in \left[t_{start} - \frac{\Delta t_1}{2} - \Delta t, t_{start} - \frac{\Delta t_1}{2} \right] \quad (5)$$

where t_{start} is the start time of the event, defined as above, $\frac{\Delta t_1}{2}$ is the temporal full width at half minimum (discussed below), and Δt is 10 s. The averaging after the hole is done analogously, and the angle $\Delta\phi$ between the two average magnetic field vectors is calculated.

The results are shown in Figure 4a, for both the solar wind and magnetosheath events. Instead of using histograms to present our statistical results, we will use Kernel Density Estimates (KDEs) (e.g., Hansen, 2005). KDEs can be thought of as a continuous version of a histogram, but give a direct estimate of the assumed, underlying probability distribution of the data samples, which are also easy to compare to fits of various assumed probability functions. In Figure 4a we also show the results in the form of histograms for comparison, but from here on we only show KDEs. We also give the means and medians for the two regions. For KDEs the amount of smoothing, which is analogous to the bin width in a histogram, is given by a

Magnetic hole magnetic field rotation

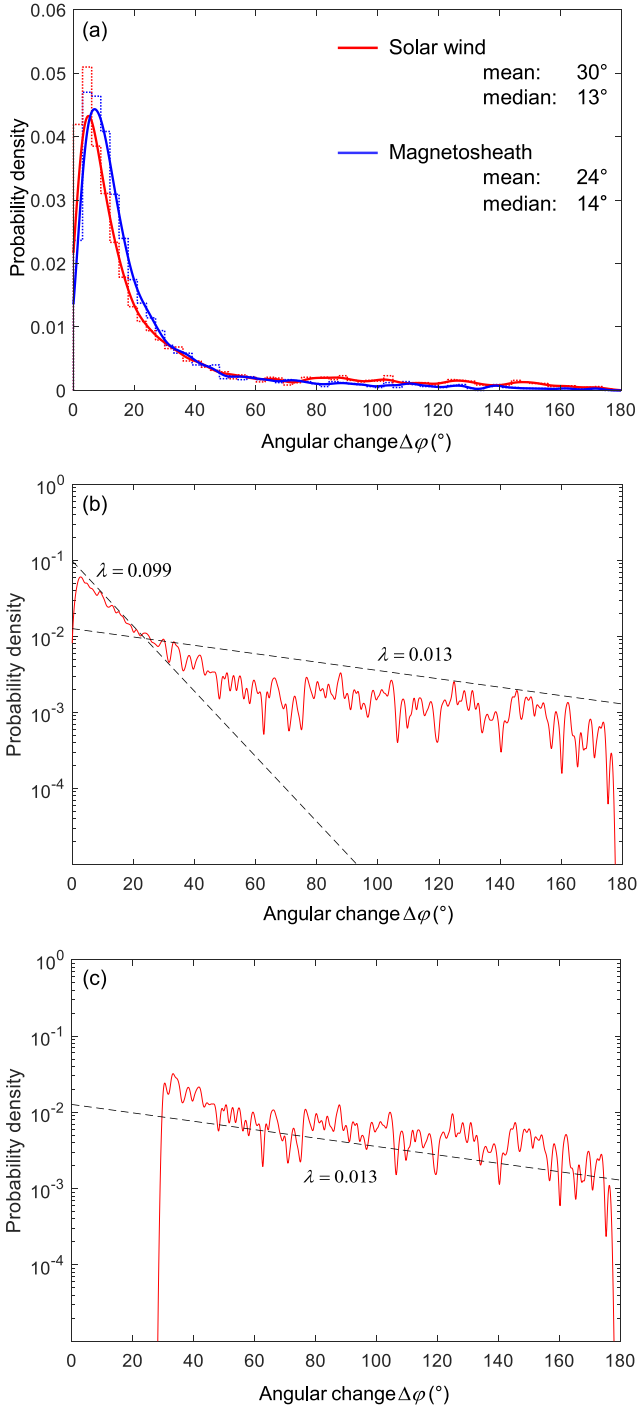


Figure 4. (a) Distributions of angular change across solar wind and magnetosheath holes, represented both as histograms and Kernel Density Estimates (KDEs), together with values of mean and median. (b) A fit of two exponential functions to the solar wind distribution represented by a KDE. (c) Fit of an exponential function to the part of the distribution with $\Delta\phi \geq 30^\circ$.

bandwidth parameter. For most KDEs presented here we choose the so-called “optimal bandwidth”, as given by Bowman and Azzalini (1997). It is clear that the distributions of the solar wind and magnetosheath holes are quite similar.

As discussed in the introduction, the classification into linear and rotational holes has been chosen rather arbitrarily. It would be desirable to have some basis for this choice. In Figure 4b we have plotted the KDE for the solar wind angular change on a logarithmic scale. We have also fitted two exponential probability distributions for lower and higher rotation angles, which have a probability density functions

$$f(\Delta\phi) = \begin{cases} \lambda e^{-\lambda\Delta\phi}, & \Delta\phi < 30^\circ, \\ 0, & \Delta\phi \geq 30^\circ, \end{cases} \quad (6)$$

$$f(\Delta\phi) = \begin{cases} 0, & \Delta\phi < 30^\circ, \\ \lambda e^{-\lambda\Delta\phi}, & \Delta\phi \geq 30^\circ, \end{cases} \quad (7)$$

respectively. The localized maximum in the KDE away from the origin is an artifact of the finite bandwidth used in the KDE calculation, which we have verified by manually varying the bandwidth. The resulting values for λ are shown in the panel (b). There is a clear indication of two different populations, with a crossover point at $\Delta\phi \simeq 25^\circ$. The fitted probability density function for the larger angular changes appears not to be well fitted to the KDE. This is an artifact due to inconsistent normalization of the KDE for the whole interval, and the part of the KDE for $\Delta\phi > 30^\circ$. It is the latter that should be compared to the fit, and we do this in panel (c) for completeness.

We suggest that a logical choice for defining the boundary between linear and rotational magnetic holes then is to choose a value of 25°. Slightly varying the chosen cutoff angles in Equations 6 and 7 gives similar results. As an example, in Figure 5 we show a magnetic hole with an angular change of $\Delta\phi = 21^\circ$. The same procedure applied on the magnetosheath magnetic hole distribution produces similar results, and we will apply the same definition there. With these definitions, the resulting number of solar wind linear magnetic holes are 1,891 (69%), with 835 rotational ones. For the magnetosheath there are 1,610 (75%) linear holes, and 544 rotational holes.

Next we show distributions of the depth of the magnetic holes, as measured by $-\frac{\Delta B}{B_0}$. The distributions for solar wind and magnetosheath mag-

netic holes are quite similar, and therefore so are the mean and medians, although the solar wind distribution is somewhat broader (Figure 6). The limited interval makes it difficult to fit a distribution, and we have refrained from doing so. In panel (b) we have plotted the distribution for linear and rotational magnetic holes separately, for both solar wind and magnetosheath magnetic holes, using the value of $\Delta\phi = 25^\circ$ to separate them. There is very little difference between the distributions. We have checked the results, also using smaller separation angles, down to 5° , with very similar results.

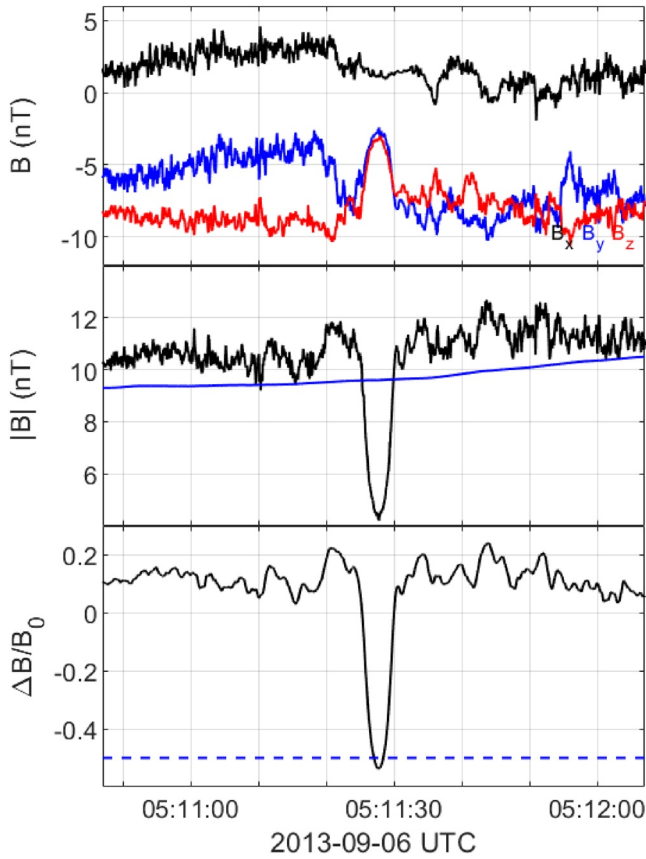


Figure 5. An example of a solar wind magnetic hole with $\Delta\phi = 21^\circ$.

It is, however, possible that a very large magnetic field rotation is needed for the magnetic holes to have different properties, for example, associated with different generation mechanisms. To investigate this, we also plot the KDE for magnetic holes with very large magnetic field rotations. We set the limit to $\Delta\phi = 140^\circ$, and call magnetic holes with a larger rotation than that “superrotational” holes (not to be confused with the same term used in, e.g., atmospheric science). It can be seen that the superrotational holes have a quite different distribution, with larger means and medians for the magnetic field depth. It is striking that the solar wind and magnetosheath magnetic holes have the same behavior in this respect. The limit of 140° is somewhat arbitrary, but it represents a value which gives a clear difference in the distribution, while retaining a reasonable number of events.

We define the temporal scale size of magnetic holes, as the full width at half minimum, applied on the time series of $\frac{\Delta B}{B_0}$. The KDEs for the solar

wind and magnetosheath are shown in Figure 7a. For both distributions, there is a maximum that is clearly separated from the origin, with the distribution probability density tending toward zero at the origin. This is an indication that the distributions may be log-normally distributed, that is, their logarithm is normally distributed. The log-normal distribution has the probability density function

$$f(x) = \begin{cases} \frac{1}{x\sigma\sqrt{2\pi}} e^{-\frac{(\ln x - \mu)^2}{2\sigma^2}}, & x \geq 0, \\ 0, & x < 0, \end{cases} \quad (8)$$

where μ is the mean of the normally distributed logarithms, and σ is the corresponding standard deviation. This translates to the mean (m) and standard deviation (s) of the log-normal distribution as

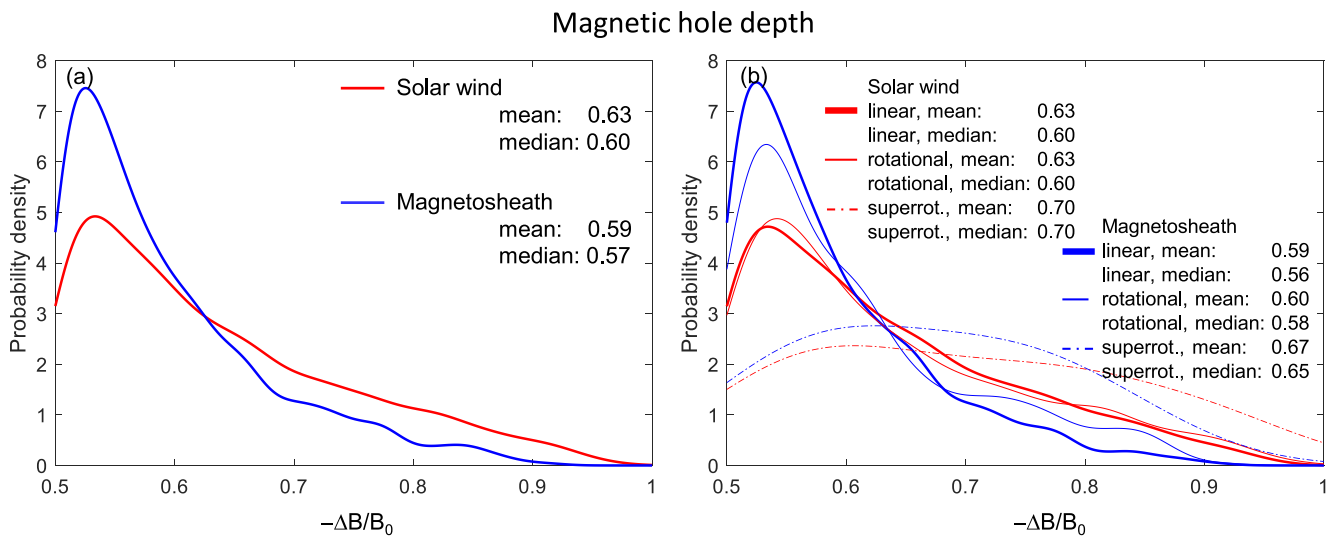


Figure 6. (a) KDEs for relative magnetic hole depth $-\frac{\Delta B}{B_0}$, for all solar wind and magnetosheath events. (b) Same as (a) but divided in linear, rotational and superrotational magnetic holes.

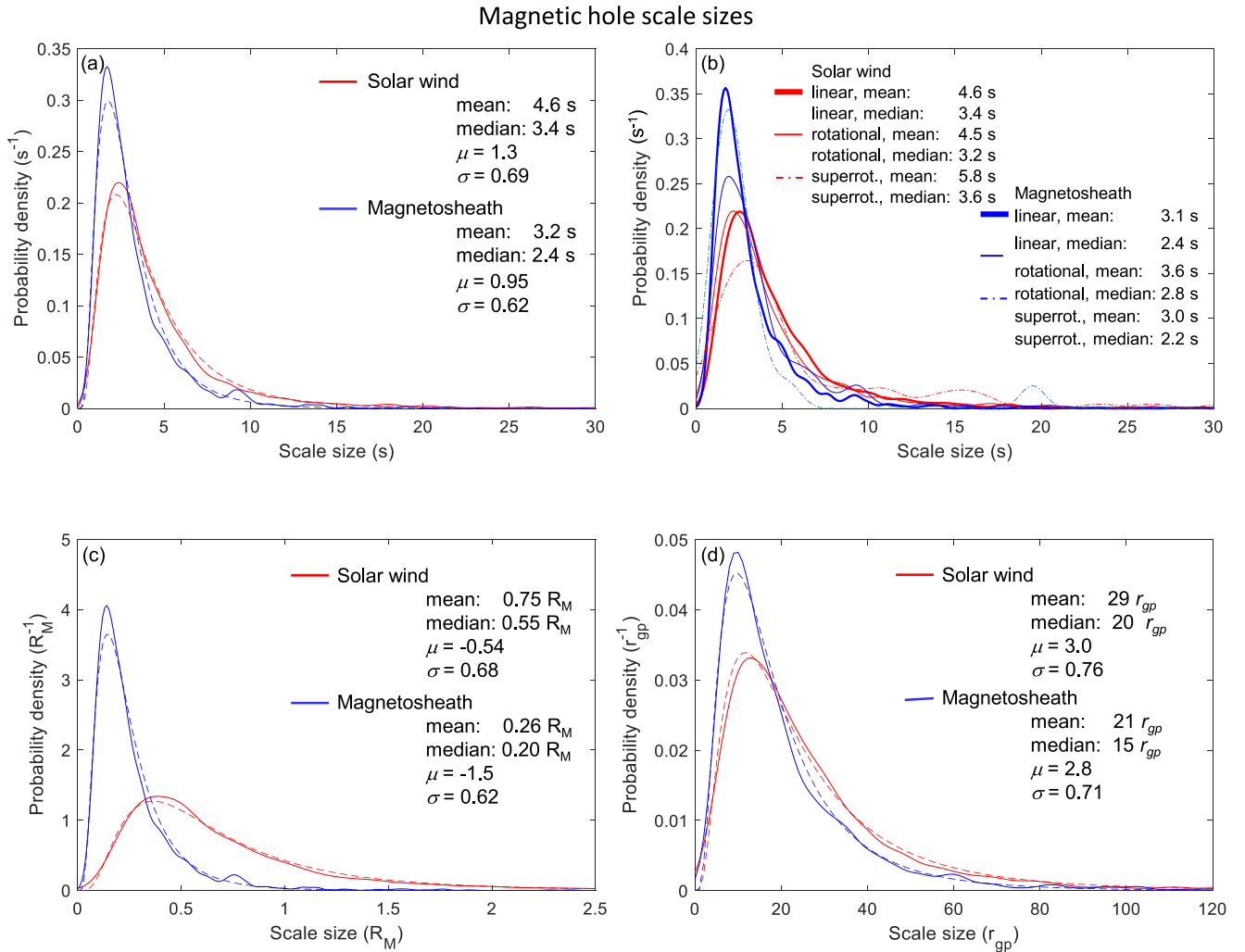


Figure 7. (a) KDEs for temporal scale size of magnetic holes in the solar wind and magnetosheath (solid line), together with fitted log-normal distributions (dashed line). (b) KDEs for magnetic holes sorted by rotational properties. (c) Same as (a), but in units of Mercury radii ($1 R_M = 2,440$ km). (d) Same as (a) but in units of thermal proton gyro radii (r_{gp}).

$$\begin{cases} m = e^{\mu + \frac{\sigma^2}{2}} \\ s = e^{\mu + \frac{\sigma^2}{2}} \sqrt{e^{\sigma^2} - 1} \end{cases} \quad (9)$$

(e.g., Blom, 1970). Fitting the KDEs with log-normal distributions, with the resulting parameters given in Figure 7a, gives a satisfactory result. Phenomena that are described by log-normal distributions are often the results of multiplicative growth or decay, and we will return to the possible importance of this later.

The distributions of the temporal scale sizes in the solar wind and magnetosheath are quite similar, which is consistent with a compression of structures crossing the bow shock. This is a consequence of the fact that the temporal scale size does not depend on the plasma flow velocity. This, in turn, can be understood in terms of the continuity equation, which in 1D states that $vn = \text{const}$, where v is the flow velocity and n is the number density. If Δl is the spatial scale size along the flow, N is the number of particles in the structure over a cross section A of the flow, $n = N/(A\Delta l)$ and therefore $vN/(A\Delta l) = \text{const}$, which means that $v/\Delta l = \text{const}$. But Δt , the temporal scale size of the structure is $\Delta l/v$, which therefore also is constant. In par-

ticular, passage across the bow shock should to first approximation conserve the temporal scale size even if the flow velocity changes dramatically, as long as this is the main effect of the interaction of the bow shock. In this way we can conclude the similarity between the two populations without information of the plasma flow velocity.

In Figure 7b, we show scale sizes for the different rotational subgroups, similar to Figure 6b. In this case, there are no significant differences for the different subgroups. In panels (c) and (d) we estimate spatial scale sizes from the temporal ones in two different ways. Since the MESSENGER plasma measurements are very limited, and cannot systematically provide flow velocities, we assume fixed flow velocities of 400 km/s for the solar wind and 200 km/s for the magnetosheath. These values are broadly consistent with values from the MHD simulations of Jia et al. (2015). We also assume that the magnetic holes are convected with the solar wind flow, and do not propagate in the solar wind frame of reference. An indication that this may be true is the result found by Karlsson et al. (2012), which showed, using Cluster multipoint data, that so called “diamagnetic plasmoids” in the magnetosheath convected with the magnetosheath flow. These plasmoids were suggested to be solar wind magnetic holes that penetrated the bow shock and entered the magnetosheath (Karlsson et al., 2015). Possible solar wind magnetic hole propagation will have to be further studied using multipoint measurements. In the meantime, the propagation velocities will likely be of the order of the local Alfvén velocity or less (e.g., Baumgärtel, 1999; Buti et al., 2001), which is comparable to the uncertainties associated with using a fixed velocity.

With these values, we can transform the temporal scale sizes to spatial ones, and the results are shown in Figure 7c (again with fitted log-normal distributions). Of course, the spatial scale sizes in the magnetosheath are shorter than in the solar wind, since the temporal scale sizes are similar. The uncertainties here are of course large, but the calculation will still give a sense of the extent of the magnetic holes compared to the magnetosphere. One way to estimate them is to use the value of the standard deviation of the solar wind velocity at 0.3 AU, which has been reported to be 90 km/s. For a solar wind velocity of 400 km/s, this corresponds to a relative uncertainty of 22%. This will also be the relative uncertainty for the magnetosheath magnetic hole scale sizes.

We can also relate the spatial scale sizes shown in panel (c) to some plasma physical parameter, for example, the proton thermal gyro radius. In order to do this, we will again have to make some assumptions, this time about the proton temperature in the solar wind and magnetosheath. We will use the averages of the temperatures estimated by Uritsky et al. (2011, Table 2), which is 40 eV for the solar wind, and 68 eV for the magnetosheath. We then use the background magnetic field B_0 (evaluated at the minimum of each magnetic hole) to calculate the ion gyro radius. The resulting KDEs for these values are shown in Figure 7d, together with the fitted log-normal distributions. Setting the uncertainty in the ion temperature to 15 eV, which is the difference between the two values of ion temperature given by Uritsky et al. (2011) and their average, we can use the error propagation formula to estimate the uncertainty in the scale size in terms of ion gyro radii. This results in an uncertainty of 23% for the solar wind values. A similar calculation for the magnetosheath values gives the same result. Setting the uncertainty of the ion energy instead to 90% of the value of the energy itself, to make a very unconservative estimate, results in a relative uncertainty of 50% for both regions.

The scale size determined by the temporal duration of the magnetic holes may depend on the orientation of the holes, if they have a non-spherical shape. Several authors have investigated the magnetic hole morphology under the assumption that they are aligned with the background magnetic field, specifically with the shape of a rotational ellipsoid. At 0.72 AU Zhang, Russell, Baumjohann, et al. (2008) found that the ratio of the scale length along the background magnetic field and perpendicular to it was 2.45:1 for linear magnetic holes. At 1 AU Xiao et al. (2010) found a ratio of 1.93:1, while at 1.5 AU Madanian et al. (2019) give a value of 1.67. We have performed a similar analysis, presented in the form of a bivariate Kernel Density Estimate with respect to scale size and the cosine of the IMF cone angle θ_c , found in Figure 8. The assumption is that the cone angle represents the angle between the IMF and the solar wind velocity, that is, that the solar wind is assumed to be directed in the negative x_{MSM} direction (We consider the solar wind aberration due to the orbital velocity of Mercury to be a small effect in the context.) No apparent dependence on the cone angle can be seen for this data set. This is consistent with a value of the Pearson correlation coefficient of -0.12 . Considering only linear or rotational holes gives correlation coefficients of -0.17 , and 0.15 , respectively. In all cases the p-value is less than 0.01. For superrotational holes the p-value is above the level of significance.

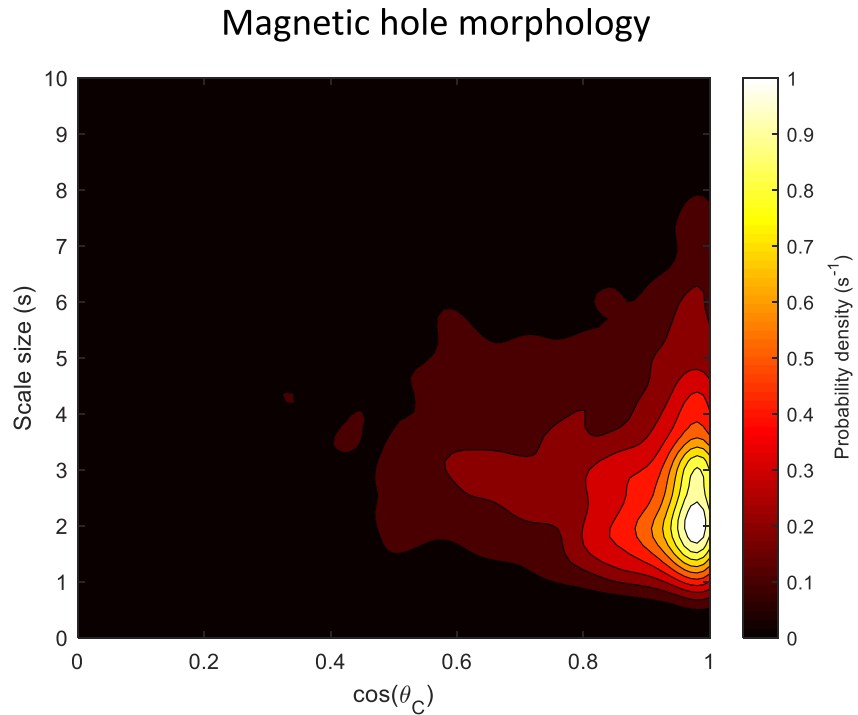


Figure 8. Bivariate Kernel Density Estimate for the scale size and cosine of the solar wind magnetic field cone angle associated with the magnetic holes.

The fact that we do not observe a dependence on θ_C is an indication that the magnetic holes at Mercury orbit either do not deviate from a spherical morphology, or that their deviation from a spherical shape is not related to the background magnetic field direction. However, this conclusion should be taken with caution, since at the orbit of Mercury the Parker angle of the solar wind is quite small, giving a mainly radial IMF for most of the time. Therefore, the data set is dominated by small values of θ_C , and a true dependence may be masked by the limited data coverage in θ_C .

In the magnetosheath, a similar analysis is difficult, since the flow velocity is less straightforward to assume. Instead we investigate the magnetic hole morphology in another way, testing the hypothesis that magnetosheath holes are solar wind holes crossing the bow shock. If this is true, and if solar wind magnetic holes have an approximately spherical or cylindrical shape, the compression of the magnetic holes as they cross the bow shock will tend to align them according to the orientation of the bow shock. This effect was shown for so-called diamagnetic plasmoids in Earth's magnetosheath (Karlsson et al., 2012), and was interpreted as the compression of solar wind magnetic holes, as described above.

To illustrate the expected effects, we have constructed a simple 2D model of how a circular structure is deformed when crossing the bow shock away from the subsolar point (The circular structure can represent a cut through a spherical, cylindrical or spheroidal structure extending out in the z direction.) Assuming a solar wind flow in the x direction and a bow shock with a normal at a certain angle (we have chosen 30°) from the x direction, we can determine the downstream flow from the Rankine-Hugonit relations. For simplicity, we take the high-Mach number limit, where (in the deHoffman-Teller frame) the tangential flow across the shock is continuous, and the normal flow is reduced by the factor $1/r$, where r is the shock compression factor (e.g., Priest, 1982). We take the maximum value of r , which is 4, and in the general case corresponds to a high Alfvén velocity in the solar wind. Assuming also that the solar wind magnetic field is parallel to the flow velocity, so that we already are in the deHoffman-Teller frame, the downstream velocity is now easily determined (we use arbitrary units). The details are not critically important, what is important is that the magnetosheath flow is considerably slower than the upstream value, and diverted away in the negative y direction.

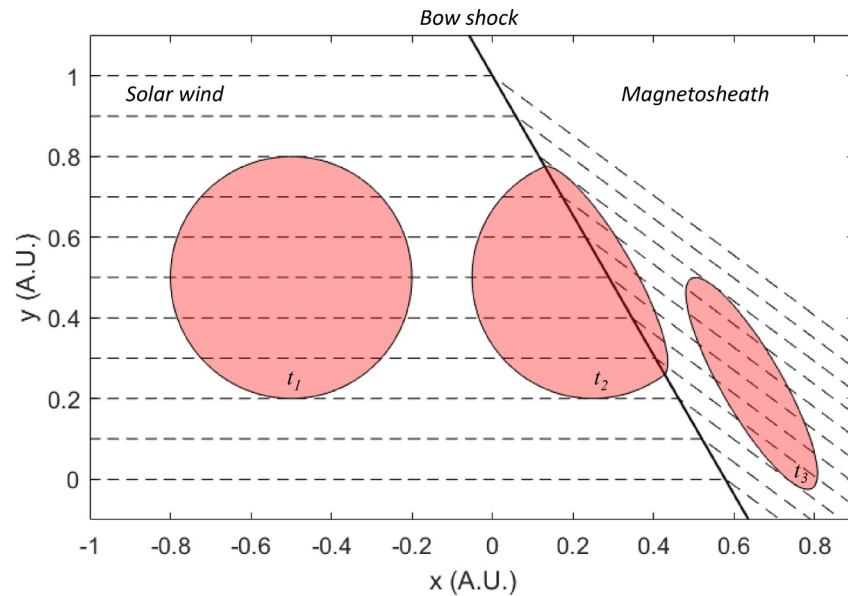


Figure 9. Simple model of the deformation of a circular structure crossing the bow shock. x and y are given in arbitrary units (A.U.).

We can now track the points on the boundary of the circular structure, assuming that they follow the plasma flow. Figure 9 shows the results at the starting time, and two later times. The braking of the leading part of the structure before the trailing one, together with the inclination of the bow shock produces two effects: a compression and an alignment of the structure to the bow shock, so that the normal taken at a large majority of the boundary of the downstream structure is close to the direction of the bow shock normal. Note that the temporal separation between the leading and trailing boundaries along a particular flow line is the same at all times.

In order to study if this effect is apparent in the observations, we consider only magnetic holes on the day side, arguing that these magnetic holes have not traveled very far after their supposed crossing of the bow shock, and will have retained their morphology. We then perform a minimum variance analysis (MVA) (Sonnerup & Scheible, 1998) on the magnetic field, across the magnetic hole structures. A minimization of the variance leads to the determination of eigenvectors to the variance matrix of the magnetic field over the MVA interval. This results in determination of the normal to an assumed one-dimensional structure, coinciding with the direction of minimum variance of the magnetic field. The vectors indicating the medium and maximum variance directions are also obtained. A well-defined determination of the minimum variance directions is often assumed if the eigenvalues corresponding to the medium and minimum variance directions have a large enough ratio. We here only use events where this ratio is larger than five.

The projections of the resulting minimum variance normal vectors in the $X_{\text{MSM}} - Y_{\text{MSM}}$ plane are plotted in panel (a) of Figure 10, where each vector is placed at the position of the corresponding magnetic hole, projected to the same plane. We have forced the normal vectors to have a negative X_{MSM} component. There is a rather strong tendency for the minimum variance directions to be directed normal to the bow shock, indicating that the magnetosheath magnetic holes have a flattened morphology, aligned with the bow shock. To quantify this correlation, we introduce two angles, θ and ϕ . θ is the angle of the radius vector of the position of the magnetic hole to the x axis (see panel [b]). This is a proxy of the direction of the bow shock normal associated with the magnetic hole. There is of course some uncertainty in relating the magnetic hole to the position where it actually crossed the bow shock, but this procedure should be enough to establish if there is any systematic behavior in the orientation of the magnetic holes. Using only dayside events should limit this uncertainty, since the magnetic holes will only be able to travel a limited distance downstream of the bow shock. We now define ϕ as the angle the MVA normal makes with the negative x direction. If the magnetic holes are oriented like in Figure 9, there should be a clear correlation between these angles. As can be seen in panel (c), this is indeed the case. The correlation coefficient is 0.65, with a p -value of less than 10^{-4}). The

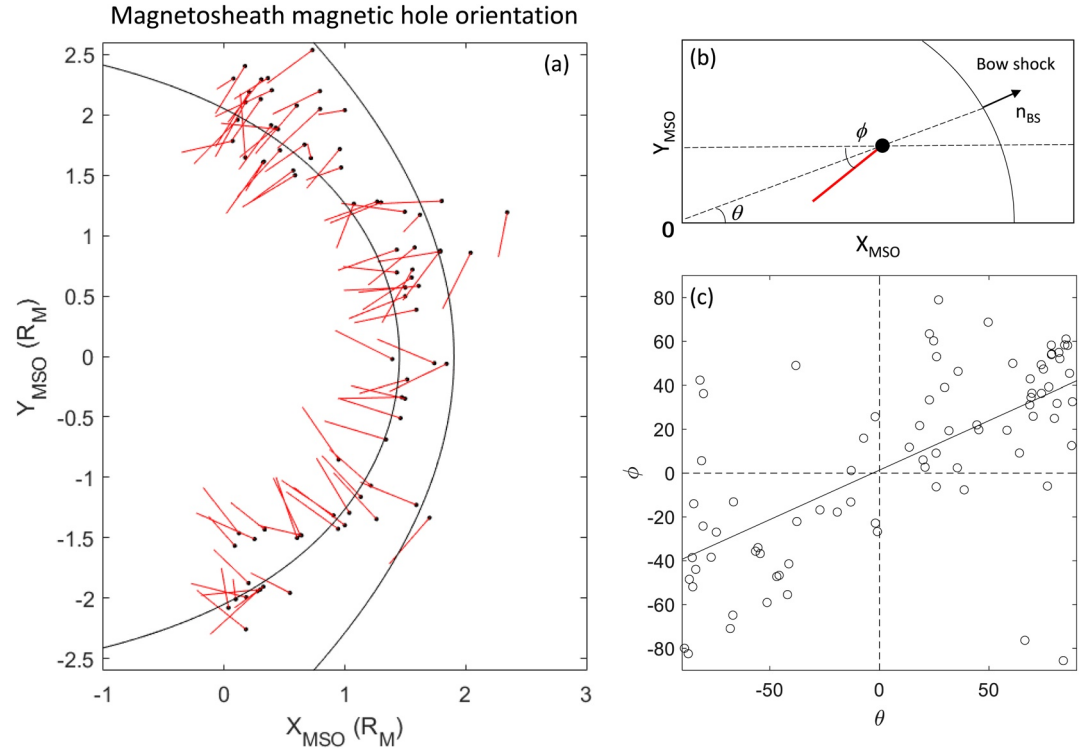


Figure 10. (a) Projection of minimum variance normals (red) on to the $X_{MSM} - Y_{MSM}$ plane, for magnetosheath magnetic holes, together with the corresponding magnetic hole positions (black). Also indicated are the statistical bow shock and magnetopause (Winslow et al., 2013). (b) Schematic, showing the definitions of the angles θ and ϕ . (c) θ versus ϕ with linear regression line.

slope is not unity, but rather around 0.5. This is perhaps not surprising since the alignment with the bow shock seen in Figure 9 is not perfect, and depends on the upstream parameters.

Finally, we want to test if solar wind magnetic holes at Mercury orbit are more common when the solar wind plasma β is higher than average. According to Equation 1, a large (perpendicular) plasma β will lead to instability for a negative temperature anisotropy ($1 - \frac{T_{\perp}}{T_{\parallel}} < 0$). Furthermore, as mentioned above, a large

β will favor magnetic mirror mode growth over ion cyclotron wave growth. In the absence of routine determination of plasma temperature and density from the particle data, we will use a low value of the magnetic field strength as a proxy for a high β . There is some circumstantial evidence that this may be valid, in the form of examples where solar wind magnetic holes (and structures of the same type not deep enough to qualify for magnetic holes in this study) are observed in isolated regions of smaller magnetic field strength. Two examples are shown in Figure 11.

In Figure 12 we show the distributions of the background magnetic field, B_0 , for magnetic holes in the solar wind and magnetosheath, sorted by rotational properties. All distributions are reasonably well fitted by log-normal distributions, as is common for positive definite natural phenomena. We here choose to show the distributions of the (natural) logarithm of B_0 , in order to more easily discuss the statistical relevance of differences in the properties of the various types of magnetic holes. The fits to normal distributions are reasonable, although a tendency for a double peak can be seen in the all mission distribution for the solar wind.

We can first note that the mean value of $\ln(B_0)$ clearly shows that linear magnetic holes have a lower B_0 than average. Using Equation 9, the corresponding magnetic field averages are 14.9 and 24.1 nT. Assuming a constant thermal pressure, this represents a difference of a factor 2.6 for the plasma β . Also the rotational magnetic holes show a lower B_0 than the average solar wind values, but with a somewhat smaller difference. The corresponding mean of B_0 is 16.3 nT.

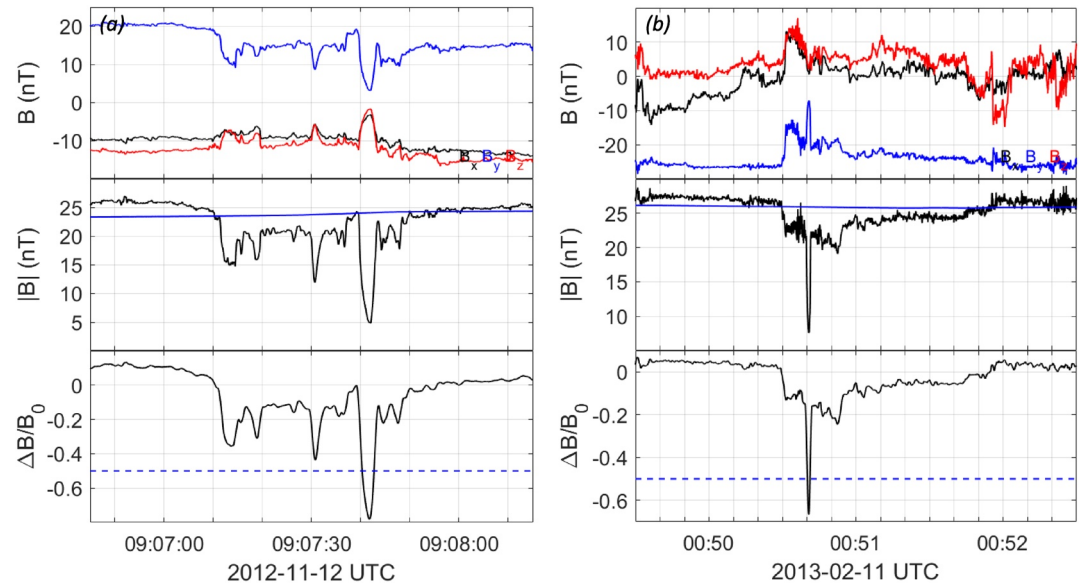


Figure 11. Two examples of regions of lower magnetic field strength (and therefore possibly higher plasma β), associated with magnetic holes and other small-scale, low-magnetic field structures.

The large sample sizes ensure that the difference in means is significant for linear and rotational magnetic holes. This is formally tested by applying the Welch t-test (e.g., Hansen et al., 2016) (because of the different sample sizes and standard deviations of the distributions), which rejects the null hypothesis that the means are equal with a p-value of less than 10^{-4} . For the superrotational magnetic holes, the difference in the mean is not significant, according to the Welch t-test.

For the magnetosheath magnetic holes, the behavior is quite different, with a very small difference in average B_0 (although, formally, statistically significant for linear and rotational magnetic holes).

4. Discussion

We will begin by discussing the properties of the solar wind magnetic holes, before turning to magnetic holes in the magnetosheath.

4.1. Solar Wind Magnetic Holes

The daily occurrence rate of solar wind magnetic holes at Mercury orbit (0.31–0.47 AU) of 4.4 d^{-1} measured here is in good agreement with the occurrence rate reported by Volwerk et al. (2020) of 4.1 d^{-1} at heliocentric distances from 0.3–0.7 AU, which we obtain by adding the rates for what they call “linear,” and “pseudo” magnetic holes, covering rotations of the magnetic field across the magnetic holes up to 45° . For our data, if we include only magnetic holes with a rotation of less than 45° , we get an occurrence rate of 3.6 d^{-1} . Our results are also broadly consistent with those of Sperveslage et al. (2000) of $1.7\text{--}2.2 \text{ d}^{-1}$ for the inner solar system (0.3–1 AU). Their lower rate may be due to differences in how magnetic holes are identified. An indication that this is the case is their result of an average magnetic hole temporal scale size of 8 s in the inner solar system, which may mean that they do not identify as many of the smaller-scale magnetic holes as we do.

The distribution of angular change of the magnetic field across solar wind magnetic holes is similar to what has been reported earlier. Sperveslage et al. (2000), for example, give an average of 23.4° between 0.3 and 1 AU, with a similar shape of the distribution (c.f. their Figure 5). Sperveslage et al. (2000) also show that 49% of all magnetic holes have an angular change of less than 10° , in the same heliocentric distance range, while Madanian et al. (2019) shows that the percentage is 51% at Mars orbit. For our data set that figure is 43%, not indicating a drastic change from 0.3 to 1.5 AU. Tsurutani et al. (2009) give an exponential fit to the angular

Background magnetic field

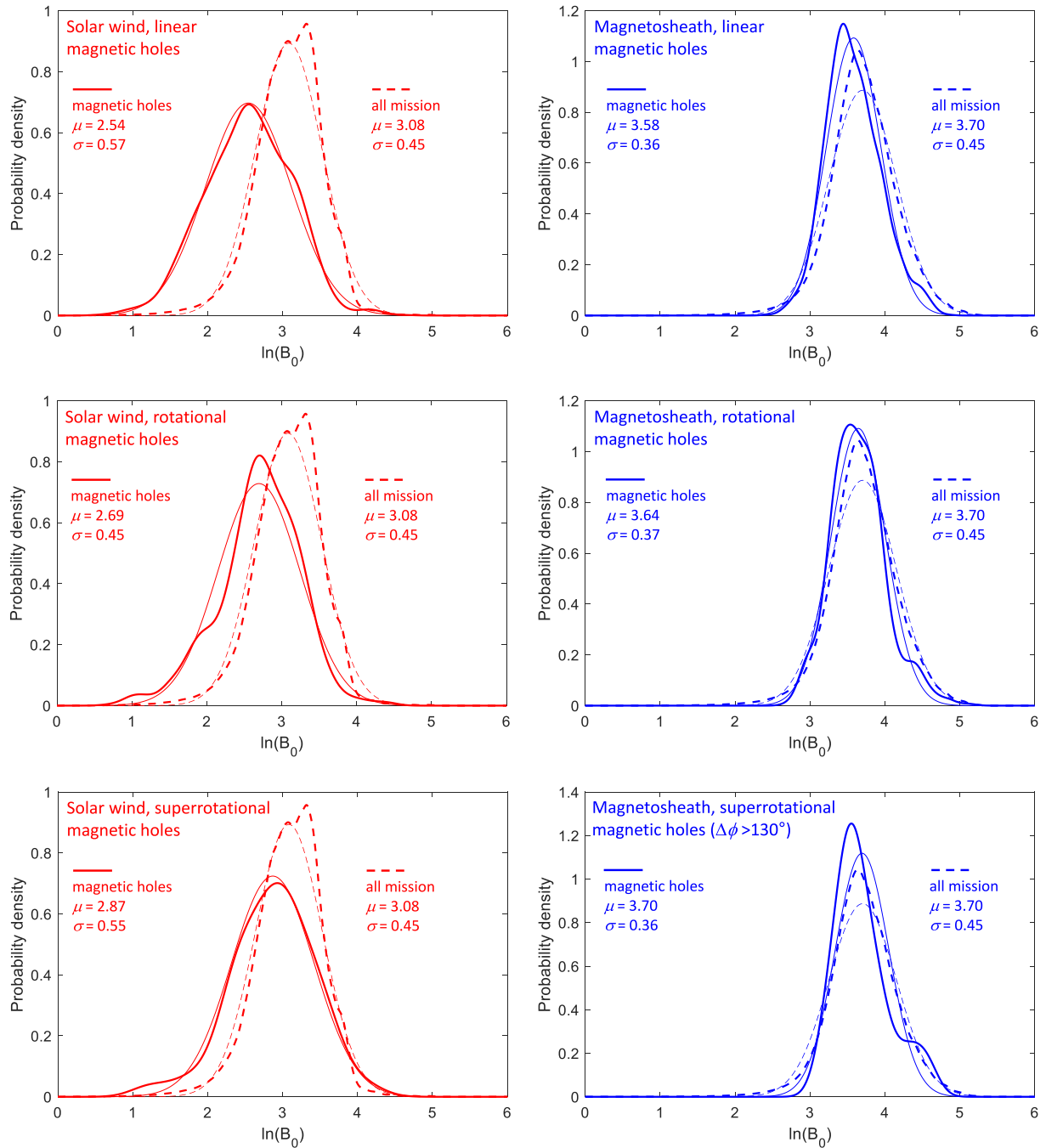


Figure 12. KDEs for the natural logarithm of the background magnetic field B_0 for magnetic holes in the solar wind and magnetosheath, divided in groups with respect to the magnetic field rotation across the magnetic holes. For each plot is shown the magnetic hole KDE with a thick solid line, and a fitted normal distribution with a thin solid line. Also shown in all plots is the KDE for the logarithm of the magnetic field for the whole MESSENGER mission (for the solar wind and magnetosheath, respectively), with a thick dashed line for the KDE and a thin dashed line for a fit to a normal distribution.

change between 1 and 5 AU, only considering angles greater than 10° , and gets a parameter corresponding to our λ of 0.05, in between the values of our two fitted values.

The definition of linear and rotational solar wind magnetic holes has been arbitrary in earlier studies. We here present some indication that there is a change in the distribution at an angle of around 25° . This may

be a natural value at which to place the limit. On the other hand, there is very little of a difference of properties between linear and rotational magnetic holes, so defined. Their distributions in magnetic hole depth, scale size, and background magnetic field B_0 are quite similar, which argues against them being generated in a different way than linear magnetic holes. Only when we consider very large rotations, the superrotational magnetic holes, do we begin to see some differences in the properties. The superrotational holes are deeper, with a larger $\Delta B/B_0$, and have no clear dependence on the background magnetic field. We can note that the increased depth of the superrotational magnetic holes is consistent with the result of Zhang, Russell, Zambelli, et al. (2008), who saw a steady increase of the depth from angular changes of around 120° , with the deepest depressions for angular changes over 150° . The different behavior of the superrotational magnetic holes may point to a different generation mechanism for this population. Although magnetic reconnection has been shown to exist even for current sheets with small rotations (Gosling, 2012; Phan et al., 2010) (and the small minimum in B_x in the rotational magnetic hole of Figure 2d could be an indication of reconnection-associated current filamentation (e.g., Che et al., 2011), even if this is not a super-rotational magnetic hole) perhaps larger magnetic shear will produce deeper magnetic holes. Furthermore Phan et al. (2010) point out that reconnection in solar wind current sheets tends to be suppressed for current sheets with small magnetic rotation in high- β regions of the solar wind. More detailed investigations of this type of magnetic hole is necessary, to for example, investigate if magnetic reconnection sometimes is active at the current sheets associated with these large magnetic field rotations. On the other hand, what has so far been called “rotational holes”, with angular changes of $10^\circ < \Delta\phi < 150^\circ$ may not be different in nature to linear magnetic holes.

The scale sizes of the solar wind magnetic holes found in this study is somewhat smaller than those given for comparable heliocentric distances by Sperveslage et al. (2000) and Volwerk et al. (2020). Tsurutani et al. (2009) give an exponential distribution of scale sizes with $\lambda = 0.059 \text{ s}^{-1}$, which gives a mean of 17 s. In the case of Tsurutani et al. (2009) this is not unexpected, since their result is based on measurements at heliocentric distances from 0.5 to 5 AU, and furthermore they use Ulysses magnetic field data with 1 s resolution, which means they will not register many of the magnetic holes found in this study. For the results of Sperveslage et al. (2000) and Volwerk et al. (2020), differences in definitions and details in the data handling may be the reason for the different results. This illustrates the need for a careful comparison between magnetic holes at different heliocentric distances with identical methodology. It seems clear, however, that the scale sizes of magnetic holes in the inner solar system are much smaller than of those further out in the solar system. A detailed comparison may reveal if this is due to expansion of magnetic holes created in the inner solar system (perhaps by Bohm diffusion, as suggested by Volwerk et al. [2020]), or if magnetic holes are continuously created as the solar wind travels outwards from the sun.

The solar wind magnetic holes scale sizes are a few tens of local, thermal gyro radii, r_{gp} . The average of 29 r_{gp} is consistent with the value of 35 r_{gp} at 0.3–0.5 AU given by Sperveslage et al. (2000, their Figure 7), given the uncertainty of our estimate. These authors also give values for larger heliocentric distances and report a weak decrease with distance. On the other hand Zhang et al. (2009) give values between 32 and 116 at 0.7 AU, which is significantly larger. These values are also based on an assumed temperature. At 1.5 AU, Madanian et al. (2019) also investigate scale sizes in units of proton gyro radius. They do not give any value for the mean, but from their Figure 4c, we can estimate that most magnetic holes have a width between 17 and 50 r_{gp} . However, they evaluate the thermal gyro radius using the magnetic field values inside the magnetic holes. This again shows the need for a systematic investigation of the variation, using consistent definitions, also with more relevant determinations of the solar wind velocity and temperature to eliminate the assumptions used so far. On the agenda is to investigate data from the Solar Orbiter and upcoming BepiColombo missions. This is of importance, since knowing how the magnetic holes scale, normalized to a physically relevant parameter, varies with heliocentric distance may reveal if magnetic holes are generated continuously in the solar wind, or are mainly transported outwards from a generation in the inner solar system.

All the solar wind magnetic holes in this study show a log-normal distribution of scale sizes. Such distributions are common in nature, in particular when the phenomena or structures in question are related to multiplicative growth or decay (e.g., Mitzenmacher, 2004). This can be understood in terms of the central limit theorem of statistics, which states that the sum of independent random variables tends to a normal distribution, even if the individual random variables are not normally distributed. Multiplicative processes

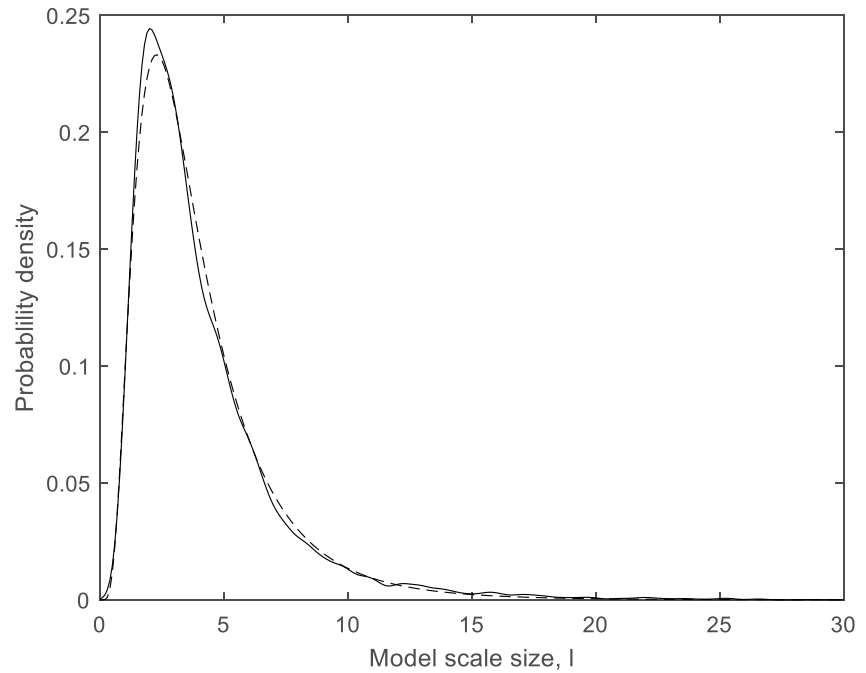


Figure 13. The resulting distribution of (dimensionless) scale sizes, l for a simple, heuristic model of the development of magnetic hole scale sizes with multiplicative growth and decay. Solid line: KDE, dashed line: fitted log-normal distribution.

correspond to additions on a logarithmic scale, and therefore lead to a normal distribution of the logarithm of the property of interest, or a log-normal distribution of the property itself. Typical examples are the size of small particles, created by coalescence of liquid particles resulting from gaseous metal (Granqvist & Buhrman, 1976), or coagulation of aerosols (Park et al., 1999). Also the opposite process of breakage, for example, creation of sand particles by crushing of rock, can result in log-normal distributions (Epstein, 1947).

We here present a simple, heuristic model to illustrate how magnetic hole scale sizes may obtain a log-normal distribution. As discussed in the introduction, magnetic holes have been suggested to be created by coalescing magnetic mirror mode structures (Winterhalter et al., 1994). Simulations by Shoji et al. (2012) have shown that such coalescence of magnetic mirror mode dips may take place as a consequence of the attraction between diamagnetic currents surrounding the dips. The fact that magnetic holes are usually found in solar wind regions marginally unstable to the mirror mode instability (Stevens & Kasper, 2007; Winterhalter et al., 1994), may also mean that they undergo alternating periods of growth and decay. If the change of size in these processes depend on the instantaneous scale size, we can model the change of scale size, l , of a magnetic hole as a number of discrete changes as follows.

Consider a set of n magnetic holes, where the scale size of the j th magnetic hole at a time t_i is l_i^j , where $j = 1, 2, \dots, n$. We initialize the distribution to be uniform, so that $l_0^j = 1$. Then let

$$l_{i+1}^j = G_i^j l_i^j, j = 1, 2, \dots, n / 2 \quad (10)$$

where G_i^j is a stochastic variable, describing a random growth factor, with a uniform probability distribution on the interval (0.9,2.0). After each time step the order of the magnetic holes in the set is randomly shuffled. Thus, in each time step half of the magnetic holes are considered to coalesce with another magnetic hole. Setting $n = 10,000$, already after three time steps, a reasonable fit of the scale size distribution of the set to a log-normal distribution can be made. Figure 10 shows the distribution after 8 times steps, together with a log-normal fit (Figure 13). After further times steps the distribution remains close to log-normal, but with a consistently increasing mean. This model should of course not be taken too seriously, and the details of how the interaction between the magnetic holes takes place needs to be specified. However, it serves as an

example of how the log-normal distribution may be generated. We also observe that a model of coalescing of magnetic holes originally close to each other of course would tend to produce isolated magnetic holes as its end state.

The relation to magnetic mirror mode structures, implied in the above model and suggested by several authors, as mentioned in the introduction, is difficult to test comprehensively due to the lack of a full set of plasma instruments on MESSENGER. However, the fact that linear and moderately rotational magnetic holes are associated with a lower B_0 , and therefore a higher β is consistent with these ideas, as argued also by Winterhalter et al. (1994) and Sperveslage et al. (2000). On the other hand, in the magnetosheaths of Earth and Jupiter, mirror mode structures in the form of holes are more often found for lower β values, while a high β is often associated with mirror mode waves in the form of peaks (Balikhin et al., 2010; Joy et al., 2006; Soucek et al., 2008). The regions of lower beta may be related to magnetic field compression at the magnetopause, and it is unclear how this is related to the solar wind observations. Both Joy et al. (2006) and Enríquez-Rivera et al. (2013) suggest that the presence of holes is related to closeness to the instability limit, rather than an explicit plasma beta dependence. This would be consistent with the results of Stevens and Kasper (2007). We intend to study the correlation between plasma β and solar wind mirror mode waves and magnetic holes in more detail, using data from the Parker Solar Probe, and Solar Orbiter spacecraft, where ion and electron instrumentation is available (McComas et al., 2016; Mueller et al., 2013).

Another indication of magnetic mirror mode origin that has been cited is the tendency for magnetic holes to be more extended along the background magnetic field, than perpendicular to it (Madanian et al., 2019; Xiao et al., 2010). The results from our study are inconclusive, as discussed above. There can be several interpretations of this. The first is that an existing correlation between scale size and cone angle is not seen because of the limited sampling of the cone angle. A second possibility is that the elongation along B_0 does not exist. Horbury and Lucek (2009) suggested that magnetic mirror mode structures may end up in a more spherical shape either during a non-linear stage of growth, or by decay when the plasma turns from mirror mode unstable to stable. We can suggest a third possibility, the coalescing of individual magnetic mirror mode structures may produce more spherical structures, depending of the preferred direction of the coalescing process. If the magnetic holes at Mercury orbit are indeed close to spherical, this is in contradiction to earlier results. All those results (and ours as well) were based on single-spacecraft measurements, with large uncertainties. We plan to address this topic again, using Cluster multi-point measurements to further study the topology of magnetic holes.

While the results for linear magnetic holes are consistent with a generation mechanism related the magnetic mirror mode instability, we will also discuss some other possible mechanisms, with a focus on what predictions from these models can be tested with this data set.

Theories describing magnetic holes in terms of solitons do not directly address the generation mechanism, rather they provide a mechanism for the magnetic holes to either propagate away from the generation region, or to persist, even if the conditions for generation are no longer fulfilled. Different soliton theories predict different propagation velocities and directions. It is not possible to test this with the data set in this study, but we have initiated a study of solar wind magnetic holes using Cluster multipoint data, where we will study this question, among other things.

Buti et al. (2001) have suggested that magnetic holes can be formed when an Alfvén wave soliton propagates almost perpendicular to the background magnetic field, with a propagation velocity comparable to the Alfvén velocity, which again will have to be tested with multi-point measurements. The authors predict that magnetic holes can be created even in the absence of an ion temperature anisotropy, and that the depth of the magnetic holes increase with β . The latter prediction is consistent with the result in this paper that magnetic holes are found in regions of lower magnetic field strength. They predict magnetic hole widths of 70–200 r_{gp} , which is somewhat greater than the mean of 29 r_{gp} , even when considering our large uncertainty. Their predicted sizes also depend on the shape of the original soliton, and the fact that the model starts with an explicit form of a soliton is also the weakness of the model. It is unclear how and if this type of solitons is created, and future observations of this type of soliton in the inner heliosphere will be needed to verify this mechanism. The observed log-normal distribution of this paper also provides some constraints on the generation and dynamics of the solitons.

Tsurutani, Dasgupta, et al. (2002) and Tsurutani, Galvan, et al. (2002) have suggested that magnetic holes observed at edges of phase-steepened Alfvén waves are created as a diamagnetic effect when the ions at the ions are heated by the ponderomotive force acting on them at the steep Alfvén wave edge. Since this edge constitutes a current sheet, this mechanism is a candidate for generation of the rotational magnetic holes, perhaps in particular for the smaller rotational angles where the current sheet does not trigger reconnection. Ulysses measurements have provided some support for this in that a small sample of events showed an increase of the ion temperatures inside the magnetic holes (Tsurutani, Dasgupta, et al., 2002). Further studies using electric field data from Solar Orbiter may enable direct evaluation of the ponderomotive force. Comparison with events at 1 AU, where several possibilities to measure the electric field exist, may answer the question, posed by the authors, if this process is ongoing as the magnetic holes travels outwards in the heliosphere. Relating to the results of this study, this mechanism may account for the difference in properties between the rotational and the super-rotational magnetic holes, while it is unclear why a lower background magnetic field should be favored.

As mention above, magnetic holes associated with a large magnetic shear may be related to reconnection processes with an associated magnetic flux annihilation (Turner et al., 1977). While Zurbuchen et al. (2001) suggests that large-scale magnetic holes can be created by reconnection close to the sun, Zhang, Russell, Zambelli, et al. (2008) suggest that rotational magnetic holes are active current sheets with ongoing slow reconnection. It is difficult to discriminate between these two possibilities here. Data from Parker Solar Probe and Solar Orbiter can be used to study if the current sheets associated with the (super)rotational holes at $0.2\text{--}0.3 R_E$ are associated with active reconnection by looking for exhaust and jets (perhaps present also in slow reconnection [Kulsrud, 2001]), and lower hybrid wave activity.

Finally, Perrone et al. (2016) have discussed magnetic holes as emergent coherent structure in solar wind turbulence. However, the examples they present typically have a $\frac{\Delta B}{B_0}$ of less than 0.1, and do not fulfill the selection criteria used in this study. Likewise, magnetic holes reported from a kinetic simulation of collisional turbulence (Roytershteyn et al., 2015) show scale sizes comparable to the electron gyro radius, which is much smaller than the magnetic holes found in this study. We do not believe that the results from these studies reproduce our observations.

4.2. Magnetosheath Magnetic Holes

We now turn our attention to the magnetic holes in the magnetosheath, where we for the first time have presented a comprehensive study of isolated magnetic holes in a planetary magnetosheath. The main question to answer regarding these magnetic holes is if they are created locally in the magnetosheath, perhaps associated with a local magnetic mirror mode instability, or if they are of solar wind origin, representing solar wind magnetic holes that have crossed the bow shock while they are convected with the solar wind plasma.

Many of the observations here are consistent with the latter alternative. The solar wind and magnetosheath magnetic holes have very similar properties, not only regarding means and medians, but also in their distributions. We quote the distributions of temporal scale sizes, magnetic field depth, and angular change in this context.

The fact that the scale sizes normalized to gyro radii are so similar may be surprising, since in general the magnetic field strength and temperature should not change in the same way when the plasma crosses the bow shock. However, the magnetic holes we detect in the magnetosheath are biased toward being observed behind a quasi-perpendicular bow shock, because of the criterion of a low level of magnetic field variance.

For a perpendicular shock, there is considerable compression of the magnetic field, which tends to decrease the gyro radius in the magnetosheath. On the other hand, the increased ion temperature behind the shock tends to increase it, and these two effects may balance each other. An alternative explanation is that non-linear effects stabilize the original instability at similar scale sizes in both regions, if the plasma is still marginally unstable to for example, the mirror mode instability. This adjustment can, however, not be very large, since it would upset the very good agreement between the temporal scales of the solar wind and magnetosheath magnetic holes. Future studies of magnetosheath magnetic holes using MMS data may shed more light on this question.

Further evidence against local generation of magnetic holes in the magnetosheath is the fact that a search for waves in the Hermean magnetosheath by Sundberg et al. (2015) showed that ion-cyclotron waves were very common, but did not identify any mirror mode structures. They interpreted this as an effect of a lower plasma β value for the Mercury magnetosheath than for other planets, since the solar wind β increases with heliocentric distance. The fact that we see no sign of a lower B_0 for magnetic holes than for the surrounding magnetosheath plasma is also consistent with no association with a local mirror mode unstable plasma.

The final argument for solar wind origin of the magnetosheath magnetic holes is their orientation, which is consistent with a compression of the magnetic holes as they cross the bow shock. However, the argument could be made that the magnetic holes are really aligned with the magnetopause, as a result of a compression against this boundary, as suggested by Horbury and Lucek (2009) for mirror modes structures in Earth's magnetosheath. Mercury's magnetosheath is too small to clearly determine if the orientation of the magnetic holes is more uniform close to the bow shock or to the magnetopause, in particular in view of the relatively small number of events with a clear MVA eigenvector separation. We again plan to use Cluster data to address this question.

The only clear argument against the solar wind origin is the larger observation rate of magnetic holes in the magnetosheath. If the Rankine-Hugoniot jump conditions are valid for magnetic holes crossing the bow shock, the ratio of magnetic field inside and outside of the holes should be preserved, at least for linear magnetic holes. However, the assumption of the shock being one-dimensional in the scale of the magnetic holes is not well fulfilled, and this could lead to a change of that ratio. This could, in turn, mean that magnetic depressions with a ratio $\frac{\Delta B}{B_0}$ just below identification criterion used here could be nudged above that threshold, and vice versa. If magnetic depressions with a lower absolute value of $\frac{\Delta B}{B_0}$ are more common, this would lead to an increased detection rate, in particular of magnetic holes with a magnetic field depth close to the identification threshold. There is some evidence of that in the magnetic hole depth distribution in Figure 6a, where the number of magnetic holes in the magnetosheath is relatively more common for values of $\frac{\Delta B}{B_0} \approx -0.5$. This problem should be further studied with kinetic simulations of the Hermean bow shock interacting with solar wind magnetic holes, and also by investigating magnetosheath magnetic holes at planets with larger bow shocks, where the jump conditions can be expected to be better satisfied on the scale length of the magnetic holes. With BepiColombo, we will also be able to determine if the mirror mode instability criterion can sometimes be fulfilled in the Hermean magnetosheath.

A critical test of the nature of magnetosheath magnetic holes is to study if they exhibit a pressure balance with respect to thermal and magnetic pressure. While the solar wind magnetic holes have been shown to fulfill such a pressure balance, as discussed in the introduction, if the magnetic holes cross the bow shock this pressure balance will generally be disturbed. This can be realized by noting that in the Rankin-Hugoniot jump conditions the increase of plasma density and temperature is well defined by the velocity jump, while the jump in magnetic field strength depends on the magnetic field orientation. Even if the jump conditions are not valid, there is no reason to expect that thermal and magnetic pressure should change in the same way when the plasma crosses the bow shock. Testing this pressure balance in the Hermean magnetosheath will have to wait until the science phase of the BepiColombo mission, when high-quality plasma measurements will be available. In the meantime, we will study the pressure balance in the Terrestrial magnetosheath, using Cluster and MMS data. We also note that if the pressure balance is disturbed by crossing the bow shock, magnetic holes that encounter the magnetopause will interact with it differently than the surrounding plasma, possibly making a noticeable impact on the magnetopause.

5. Summary

We have presented a large statistical investigation of solar wind magnetic holes at Mercury orbit. The main results are:

1. We have found 2,726 solar wind magnetic holes, corresponding to an occurrence rate of 4.4 d^{-1} .

2. The magnetic field angular change, or rotation, across the magnetic holes follows an exponential distribution. There is an indication of two different populations with a breaking point at around 25°.
3. The distribution of magnetic hole depth is very similar for linear and rotational magnetic holes, while superrotational magnetic holes ($\Delta\phi > 140^\circ$) are shifted toward larger depths, possibly indicating a different generation mechanism for the latter.
4. The scale sizes of magnetic holes follow a log-normal distribution for both linear and rotational holes, indicating a multiplicative growth process. The mean size is estimated to be around $0.73 R_M$, or $29 r_{gp}$. We find no dependence of the scale size on the direction of the background magnetic field.
5. Solar wind magnetic holes are found in regions of lower background magnetic field than the solar wind average, which indicates that they appear in regions of higher plasma β . This is consistent with an association to the mirror mode instability, but does not unambiguously rule out other generation mechanisms.

We have also performed a comprehensive statistical investigation of magnetic holes in the Hermean magnetosheath, with the following main results:

1. We have found 2,154 magnetosheath magnetic holes, corresponding to an occurrence rate of 17 d^{-1} .
2. The distributions of angular change, magnetic field depth, and temporal scale sizes are very similar to the solar wind magnetic holes distributions, including the dependence on the two latter properties on angular rotation.
3. The magnetosheath magnetic holes are found in regions with the same background magnetic field as the magnetosheath average.
4. Magnetic holes with a clear MVA normal are found to be oriented along the bow shock or magnetopause.
5. We suggest that the origin of magnetosheath magnetic holes is most likely the solar wind, rather than local generation in the magnetosheath.

Data Availability Statement

We have used the data set MESS-E/V/H/SW-MAG-3-CDR-CALIBRATED-V1.0. D.H. was supported by the German Ministerium für Wirtschaft und Energie and the German Zentrum für Luft- und Raumfahrt under contract 50 QW 1501. C.G. is supported by an ESA research fellowship.

Acknowledgments

We are grateful to B. J. Anderson, H. Korth, J. M. Raines, and J. A. Slavin of the MESSENGER team for help with using the data set. The data used in this study can be found at the Planetary Data System (PDS): <https://pds.nasa.gov/>.

References

- Anderson, B. J., Acuña, M. H., Lohr, D. A., Scheifele, J., Raval, A., Korth, H., et al. (2007). The magnetometer instrument on messenger Space Science Reviews. In *The messenger mission to mercury* (Vol. 131, pp. 417–450). Springer. <https://doi.org/10.1007/s11214-007-9246-7>
- Avinash, K., & Zank, G. (2007). Magnetic structures in the heliosheath. *Geophysical Research Letters*, *34*(5). <https://doi.org/10.1029/2006gl028582>
- Balikhin, M., Pokhotelov, O., Walker, S., Boynton, R., & Beloff, N. (2010). Mirror mode peaks: Themis observations versus theories. *Geophysical Research Letters*, *37*(5). <https://doi.org/10.1029/2009gl042090>
- Baumgärtel, K. (1999). Soliton approach to magnetic holes. *Journal of Geophysical Research*, *104*(A12), 28295–28308. <https://doi.org/10.1029/1999ja900393>
- Blom, G. (1970). *Sannolikheteori och statistikteori med tillämpningar*. Studentlitteratur.
- Bowman, A. W., & Azzalini, A. (1997). *Applied smoothing techniques for data analysis: The Kernel approach with S-Plus illustrations* (Vol. 18). OUP Oxford.
- Briand, C., Soucek, J., Henri, P., & Mangeney, A. (2010). Waves at the electron plasma frequency associated with solar wind magnetic holes: Stereo/cluster observations. *Journal of Geophysical Research*, *115*(A12). <https://doi.org/10.1029/2010ja015849>
- Buti, B., Tsurutani, B. T., Neugebauer, M., & Goldstein, B. E. (2001). Generation mechanism for magnetic holes in the solar wind. *Geophysical Research Letters*, *28*(7), 1355–1358. <https://doi.org/10.1029/2000gl012592>
- Che, H., Drake, J. F., & Swisdak, M. (2011). A current filamentation mechanism for breaking magnetic field lines during reconnection. *Nature*, *474*(7350), 184–187. <https://doi.org/10.1038/nature10091>
- Chisham, G., Schwartz, S. J., Balikhin, M. A., & Dunlop, M. W. (1999). Amplitude observations of mirror mode waves in the magnetosheath: Wavevector determination. *Journal of Geophysical Research*, *104*(A1), 437–447. <https://doi.org/10.1029/1998ja900044>
- Enriquez-Rivera, O., Blanco-Cano, X., Russell, C. T., Jian, L. K., Luhmann, J. G., Simunac, K. D. C., et al. (2013). Mirror-mode storms inside stream interaction regions and in the ambient solar wind: A kinetic study. *Journal of Geophysical Research: Space Physics*, *118*(1), 17–28. <https://doi.org/10.1029/2012ja018233>
- Epstein, B. (1947). The mathematical description of certain breakage mechanisms leading to the logarithmic-normal distribution. *Journal of the Franklin Institute*, *244*(6), 471–477. [https://doi.org/10.1016/0016-0032\(47\)90465-1](https://doi.org/10.1016/0016-0032(47)90465-1)
- Gosling, J. (2012). Magnetic reconnection in the solar wind. *Space Science Reviews*, *172*(1–4), 187–200. <https://doi.org/10.1007/s11214-011-9747-2>
- Granqvist, C. G., & Buhrman, R. A. (1976). Log-normal size distributions of ultrafine metal particles. *Solid State Communications*, *18*(1), 123–126. [https://doi.org/10.1016/0038-1098\(76\)91415-0](https://doi.org/10.1016/0038-1098(76)91415-0)

- Grib, S. A., & Leora, S. N. (2015). The magnetic hole as plasma inhomogeneity in the solar wind and related interplanetary medium perturbations. *Geomagnetism and Aeronomy*, 55(2), 158–165. <https://doi.org/10.1134/s001679321502005x>
- Hansen, K. C., Altwegg, K., Berthelier, J.-J., Bieler, A., Biver, N., Bockelée-Morvan, D., et al. (2016). Evolution of water production of 67P/Churyumov-Gerasimenko: An empirical model and a multi-instrument study. *Monthly Notices of the Royal Astronomical Society*, 462, S491–S506. <https://doi.org/10.1093/mnras/stw2413>
- Hansen, N. R. (2005). *Probability theory and statistics*. University of Copenhagen.
- Hasegawa, A. (1969). Drift mirror instability in the magnetosphere. *Physics of Fluids*, 12(12), 2642–2650. <https://doi.org/10.1063/1.1692407>
- Horbury, T., & Lucek, E. (2009). Size, shape, and orientation of magnetosheath mirror mode structures. *Journal of Geophysical Research: Space Physics*, 114(A5). <https://doi.org/10.1029/2009ja014068>
- Jarvinen, R., Alho, M., Kallio, E., & Pulkkinen, T. I. (2019). Ultra-low-frequency waves in the ion foreshock of mercury: A global hybrid modeling study. *Monthly Notices of the Royal Astronomical Society*, 491(3), 4147–4161. <https://doi.org/10.1093/mnras/stz3257>
- Jia, X., Slavin, J. A., Gombosi, T. I., Daldorff, L. K. S., Toth, G., & Holst, B. (2015). Global MHD simulations of Mercury's magnetosphere with coupled planetary interior: Induction effect of the planetary conducting core on the global interaction. *Journal of Geophysical Research: Space Physics*, 120(6), 4763–4775. <https://doi.org/10.1002/2015ja021143>
- Joy, S., Kivelson, M., Walker, R., Khurana, K., Russell, C., & Paterson, W. (2006). Mirror mode structures in the Jovian magnetosheath. *Journal of Geophysical Research: Space Physics*, 111(A12). <https://doi.org/10.1029/2006ja011985>
- Karlsson, T., Brenning, N., Nilsson, H., Trotignon, J.-G., Vallières, X., & Facsko, G. (2012). Localized density enhancements in the magnetosheath: Three-dimensional morphology and possible importance for impulsive penetration. *Journal of Geophysical Research: Space Physics*, 117(A3). <https://doi.org/10.1029/2011ja017059>
- Karlsson, T., Kullen, A., Liljeblad, E., Brenning, N., Nilsson, H., Gunell, H., et al. (2015). On the origin of magnetosheath plasmoids and their relation to magnetosheath jets. *Journal of Geophysical Research: Space Physics*, 120, 7390–7403. <https://doi.org/10.1002/2015JA021487>
- Karlsson, T., Liljeblad, E., Kullen, A., Raines, J. M., Slavin, J. A., & Sundberg, T. (2016). Isolated magnetic field structures in Mercury's magnetosheath as possible analogues for terrestrial magnetosheath plasmoids and jets. *Planetary and Space Science*, 129, 61–73. <https://doi.org/10.1016/j.pss.2016.06.002>
- Kulsrud, R. M. (2001). Magnetic reconnection: Sweet-parker versus petschek. *Earth Planets and Space*, 53(6), 417–422. <https://doi.org/10.1186/bf03353251>
- Le, G., Chi, P. J., Blanco-Cano, X., Boardsen, S., Slavin, J. A., Anderson, B. J., et al. (2013). Upstream ultra-low frequency waves in Mercury's foreshock region: MESSENGER magnetic field observations. *Journal of Geophysical Research: Space Physics*, 118(6), 2809–2823. <https://doi.org/10.1002/jgra.50342>
- Madanian, H., Halekas, J. S., Mazelle, C. X., Omid, N., Easley, J. R., Mitchell, D. L., et al. (2019). Magnetic holes upstream of the martian bow shock: Maven observations. *Journal of Geophysical Research: Space Physics*, 125, e2019JA027198.
- McComas, D., Alexander, N., Angold, N., Bale, S., Beebe, C., Birdwell, B., et al. (2016). Integrated science investigation of the sun (isis): Design of the energetic particle investigation. *Space Science Reviews*, 204(1–4), 187–256. <https://doi.org/10.1007/s11214-014-0059-1>
- Mitzenmacher, M. (2004). A brief history of generative models for power law and lognormal distributions. *Internet Mathematics*, 1(2), 226–251. <https://doi.org/10.1080/15427951.2004.10129088>
- Mueller, D., Marsden, R. G., Cyr, O. S., Gilbert, H. R., & The Solar Orbiter Team (2013). Solar orbiter. *Solar Physics*, 285(1–2), 25–70.
- Neugebauer, M., Goldstein, B. E., Winterhalter, D., Smith, E. J., MacDowall, R. J., & Gary, S. P. (2001). Ion distributions in large magnetic holes in the fast solar wind. *Journal of Geophysical Research*, 106(A4), 5635–5648. <https://doi.org/10.1029/2000ja000331>
- Park, S. H., Lee, K. W., Otto, E., & Fissan, H. (1999). The log-normal size distribution theory of brownian aerosol coagulation for the entire particle size range. *Journal of Aerosol Science*, 30(1), 3–16. [https://doi.org/10.1016/s0021-8502\(98\)00037-8](https://doi.org/10.1016/s0021-8502(98)00037-8)
- Parkhomov, V., Eselevich, V., Eselevich, M., Dmitriev, A., & Vedernikova, T. (2019). Diamagnetic plasmoids as part of diamagnetic structures of the slow solar wind and their impact on earth's magnetosphere. *Solar-Terrestrial Physics*, 5(4), 34–45.
- Perrone, D., Alexandrova, O., Mangeney, A., Maksimovic, M., Lacombe, C., Rakoto, V., et al. (2016). Compressive coherent structures at ion scales in the slow solar wind. *Acta Pathologica Japonica*, 826(2), 196. <https://doi.org/10.3847/0004-637x/826/2/196>
- Perrone, D., Alexandrova, O., Roberts, O. W., Lion, S., Lacombe, C., Walsh, A., et al. (2017). Coherent Structures at Ion Scales in Fast Solar Wind: Cluster Observations. *Acta Pathologica Japonica*, 849(1), 49. <https://doi.org/10.3847/1538-4357/aa9022>
- Phan, T. D., Gosling, J. T., Paschmann, G., Pasma, C., Drake, J. F., Øieroset, M., et al. (2010). The dependence of magnetic reconnection on plasma β and magnetic shear: Evidence from solar wind observations. *Acta Pathologica Japonica*, 719(2), L199–L203. <https://doi.org/10.1088/2041-8205/719/2/1199>
- Philpott, L., Johnson, C., Anderson, B., & Winslow, R. (2020). The shape of mercury's magnetopause: The picture from messenger magnetometer observations and future prospects for bepicolombo. *Journal of Geophysical Research: Space Physics*, 125, e2019JA027544.
- Plaschke, F., Hietala, H., Archer, M., Blanco-Cano, X., Kajdič, P., Karlsson, T., et al. (2018). Jets downstream of collisionless shocks. *Space Science Reviews*, 214(5), 81. <https://doi.org/10.1007/s11214-018-0516-3>
- Plaschke, F., Karlsson, T., Götz, C., Möstl, C., Richter, I., Volwerk, M., et al. (2018). First observations of magnetic holes deep within the coma of a comet. *Astronomy & Astrophysics*, 618, A114. <https://doi.org/10.1051/0004-6361/201833300>
- Raines, J. M., Slavin, J. A., Zurbuchen, T. H., Gloeckler, G., Anderson, B. J., Baker, D. N., et al. (2011). Messenger observations of the plasma environment near mercury. *Planetary and Space Science*, 59(15), 2004–2015. <https://doi.org/10.1016/j.pss.2011.02.004>
- Roytershteyn, V., Karimabadi, H., & Roberts, A. (2015). Generation of magnetic holes in fully kinetic simulations of collisionless turbulence. *Philosophical Transactions of The Royal Society A*, 373(2041), 20140151. <https://doi.org/10.1098/rsta.2014.0151>
- Schwartz, S., Burgess, D., & Moses, J. (1997). Low-frequency waves in the earth's magnetosheath: Present status. *Annales Geophysicae*, 14, 1134–1150.
- Shoji, M., Omura, Y., & Lee, L.-C. (2012). Multidimensional nonlinear mirror-mode structures in the earth's magnetosheath. *Journal of Geophysical Research*, 117(A8). <https://doi.org/10.1029/2011ja017420>
- Sonnerup, B. U., & Scheible, M. (1998). Minimum and maximum variance analysis. *Analysis Methods for Multi-Spacecraft Data*, 1, 185–220.
- Soucek, J., Lucek, E., & Dandouras, I. (2008). Properties of magnetosheath mirror modes observed by cluster and their response to changes in plasma parameters. *Journal of Geophysical Research*, 113(A4). <https://doi.org/10.1029/2007ja012649>
- Southwood, D. J., & Kivelson, M. G. (1993). Mirror instability: 1. Physical mechanism of linear instability. *Journal of Geophysical Research*, 98(A6), 9181–9187. <https://doi.org/10.1029/92ja02837>
- Sperveslage, K., Neubauer, F. M., Baumgärtel, K., & Ness, N. F. (2000). Magnetic holes in the solar wind between 0.3 au and 17 au. *Nonlinear Processes in Geophysics*, 7(3/4), 191–200. <https://doi.org/10.5194/npg-7-191-2000>
- Stasiewicz, K., Shukla, P., Gustafsson, G., Buchert, S., Lavraud, B., Thidé, B., et al. (2003). Slow magnetosonic solitons detected by the cluster spacecraft. *Physical Review Letters*, 90(8), 085002. <https://doi.org/10.1103/physrevlett.90.085002>

- Stevens, M., & Kasper, J. (2007). A scale-free analysis of magnetic holes at 1 au. *Journal of Geophysical Research: Space Physics*, 112(A5). <https://doi.org/10.1029/2006ja012116>
- Sundberg, T., Boardsen, S. A., Burgess, D., & Slavin, J. A. (2015). Coherent wave activity in Mercury's magnetosheath. *Journal of Geophysical Research: Space Physics*, 120(9), 7342–7356. <https://doi.org/10.1002/2015ja021499>
- Sundberg, T., Boardsen, S. A., Slavin, J. A., Uritsky, V. M., Anderson, B. J., Korth, H., et al. (2013). Cyclic reformation of a quasi-parallel bow shock at mercury: Messenger observations. *Journal of Geophysical Research: Space Physics*, 118(10), 6457–6464. <https://doi.org/10.1002/jgra.50602>
- Tsurutani, B., Dasgupta, B., Galvan, C., Neugebauer, M., Lakhina, G., Arballo, J., et al. (2002). Phase-steepened Alfvén waves, proton perpendicular energization and the creation of magnetic holes and magnetic decreases: The ponderomotive force. *Geophysical Research Letters*, 29(24), 86-1–86-4. <https://doi.org/10.1029/2002gl015652>
- Tsurutani, B., Galvan, C., Arballo, J., Winterhalter, D., Sakurai, R., Smith, E., et al. (2002). Relationship between discontinuities, magnetic holes, magnetic decreases, and nonlinear Alfvén waves: Ulysses observations over the solar poles. *Geophysical Research Letters*, 29(11), 23-1–23-4. <https://doi.org/10.1029/2001gl013623>
- Tsurutani, B. T., Guarnieri, F. L., Echer, E., Lakhina, G. S., & Verkhoglyadova, O. P. (2009). Magnetic decrease formation from 1 AU to 5 AU: Corotating interaction region reverse shocks. *Journal of Geophysical Research*, 114(A8). <https://doi.org/10.1029/2008ja013927>
- Tsurutani, B. T., Lakhina, G. S., Verkhoglyadova, O. P., Echer, E., Guarnieri, F. L., Narita, Y., et al. (2011). Magnetosheath and heliosheath mirror mode structures, interplanetary magnetic decreases, and linear magnetic decreases: Differences and distinguishing features. *Journal of Geophysical Research*, 116(A2). <https://doi.org/10.1029/2010ja015913>
- Turner, J. M., Burlaga, L. F., Ness, N. F., & Lemaire, J. F. (1977). Magnetic holes in the solar wind. *Journal of Geophysical Research*, 82(13), 1921–1924. <https://doi.org/10.1029/ja082i013p01921>
- Uritsky, V., Slavin, J., Khazanov, G., Donovan, E., Boardsen, S., Anderson, B., et al. (2011). Kinetic-scale magnetic turbulence and finite Larmor radius effects at mercury. *Journal of Geophysical Research*, 116(A9). <https://doi.org/10.1029/2011ja016744>
- Volwerk, M., Goetz, C., Plaschke, F., Karlsson, T., Heyner, D., & Anderson, B. (2020). On the magnetic characteristics of magnetic holes in the solar wind between Mercury and Venus. *Annales Geophysicae*, 38, 51–60. <https://doi.org/10.5194/angeo-38-51-2020>
- Volwerk, M., Zhang, T., Delva, M., Vörös, Z., Baumjohann, W., & Glassmeier, K.-H. (2008). First identification of mirror mode waves in Venus' magnetosheath? *Geophysical Research Letters*, 35(12). <https://doi.org/10.1029/2008gl033621>
- Winslow, R. M., Anderson, B. J., Johnson, C. L., Slavin, J. A., Korth, H., Purucker, M. E., et al. (2013). Mercury's magnetopause and bow shock from MESSENGER Magnetometer observations. *Journal of Geophysical Research: Space Physics*, 118(5), 2213–2227. <https://doi.org/10.1002/jgra.50237>
- Winterhalter, D., Neugebauer, M., Goldstein, B. E., Smith, E. J., Bame, S. J., & Balogh, A. (1994). ULYSSES field and plasma observations of magnetic holes in the solar wind and their relation to mirror-mode structures. *Journal of Geophysical Research*, 99, 23371. <https://doi.org/10.1029/94JA01977>
- Wu, B. H., Mandt, M. E., Lee, L. C., & Chao, J. K. (1993). Magnetospheric response to solar wind dynamic pressure variations: Interaction of interplanetary tangential discontinuities with the bow shock. *Journal of Geophysical Research*, 98(A12), 21297–21311. <https://doi.org/10.1029/93ja01013>
- Xiao, T., Shi, Q. Q., Zhang, T. L., Fu, S. Y., Li, L., Zong, Q. G., et al. (2010). Cluster-c1 observations on the geometrical structure of linear magnetic holes in the solar wind at 1 au. *Annals of Geophysics*, 28(9), 1695–1702. <https://doi.org/10.5194/angeo-28-1695-2010>
- Zhang, T., Baumjohann, W., Russell, C., Jian, L., Wang, C., Cao, J., et al. (2009). Mirror mode structures in the solar wind at 0.72 au. *Journal of Geophysical Research*, 114(A10). <https://doi.org/10.1029/2009ja014103>
- Zhang, T., Russell, C., Baumjohann, W., Jian, L., Balikhin, M., Cao, J., et al. (2008). Characteristic size and shape of the mirror mode structures in the solar wind at 0.72 au. *Geophysical Research Letters*, 35(10). <https://doi.org/10.1029/2008gl033793>
- Zhang, T., Russell, C., Zambelli, W., Vörös, Z., Wang, C., Cao, J., et al. (2008). Behavior of current sheets at directional magnetic discontinuities in the solar wind at 0.72 au. *Geophysical Research Letters*, 35(24). <https://doi.org/10.1029/2008gl036120>
- Zurbuchen, T. H., Hefli, S., Fisk, L. A., Gloeckler, G., Schwadron, N. A., Smith, C. W., et al. (2001). On the origin of microscale magnetic holes in the solar wind. *Journal of Geophysical Research*, 106(A8), 16001–16010. <https://doi.org/10.1029/2000ja000119>